

PAPER • OPEN ACCESS

Overview of L- to H-mode transition experiments at ASDEX Upgrade

To cite this article: U Plank *et al* 2023 *Plasma Phys. Control. Fusion* **65** 014001

View the [article online](#) for updates and enhancements.

You may also like

- [Dynamics of L–H transition and I-phase in EAST](#)
G.S. Xu, H.Q. Wang, M. Xu et al.
- [The role of turbulence–flow interactions in L- to H-mode transition dynamics: recent progress](#)
L. Schmitz
- [L–H power threshold studies in JET with Be/W and C wall](#)
C.F. Maggi, E. Delabie, T.M. Biewer et al.

Overview of L- to H-mode transition experiments at ASDEX Upgrade

U Plank^{1,*} , R M McDermott¹ , G Birkenmeier¹ , N Bonanomi¹ , M Cavedon² ,
G D Conway¹ , T Eich¹ , M Griener¹ , O Grover¹ , P A Schneider¹ ,
M Willensdorfer¹  and the ASDEX Upgrade Team³

¹ Max-Planck-Institut für Plasmaphysik, Boltzmannstraße 2, Garching, 85748, Germany

² Dipartimento di Fisica ‘G. Occhialini’, Università di Milano-Bicocca, 20126 Milano, Italy

E-mail: Ulrike.Plank@ipp.mpg.de

Received 25 August 2022, revised 21 October 2022

Accepted for publication 16 November 2022

Published 6 December 2022



CrossMark

Abstract

This paper presents an overview of results from L–H transition experiments that were performed at ASDEX Upgrade (AUG) with the aim of identifying the underlying mechanisms leading to H-mode confinement. With a broad variety of experiments and new diagnostic techniques, as well as modeling efforts, AUG has contributed substantially to improving our understanding of the L–H transition over the past years. In this review, the important roles of the ion heat channel and the edge radial electric field (E_r) in the L–H transition physics are brought into context with known dependencies of the H-mode power threshold (P_{LH}), such as the impact of wall material, magnetic perturbations, and the magnetic configuration. Furthermore, experimental and theoretical results obtained at AUG on the L-mode edge turbulence are connected to the mean-field E_r and its related shear flow. This led to a deeper understanding of the I-phase plasma regime, has resolved the so-called isotope effect of P_{LH} , and led to the development of a semi-analytical model that can describe AUG’s experimental observations of the L–H transition together with the L- and H-mode density limits.

Keywords: overviews, L–H transition, ASDEX Upgrade

(Some figures may appear in colour only in the online journal)

1. Introduction

The discovery of the high confinement mode, or H-mode, and its associated improved particle and energy confinement provided a viable path to building energy-producing tokamak reactors. Since then, most reactor designs assume

H-mode level plasma confinement [1–3]. Access to H-mode has, empirically, been observed above a certain applied power level, known as the H-mode power threshold (P_{LH}). P_{LH} has been found to depend on several local and global plasma parameters, such as the plasma density, the magnetic field strength, the main ion species, the wall and divertor condition and magnetic configuration [4, 5], amongst others.

A wide variety of theories and empirical scalings have been developed (see [4, 6] and references therein), but a conclusive understanding of the fundamental physics mechanisms behind the transition from L-mode into H-mode (L–H transition) has not been obtained. This makes extrapolations of the H-mode onset to future machines challenging, because these will operate in parameter spaces very different from those in present day devices. Therefore, a more robust physics-based

³ See Stroth *et al* (2022) (<https://doi.org/10.1088/1741-4326/ac207f>) for the ASDEX Upgrade Team.

* Author to whom any correspondence should be addressed.



Original Content from this work may be used under the terms of the [Creative Commons Attribution 4.0 licence](https://creativecommons.org/licenses/by/4.0/). Any further distribution of this work must maintain attribution to the author(s) and the title of the work, journal citation and DOI.

understanding of the L–H transition is crucial to predict the H-mode access and performance of future fusion reactors correctly.

ASDEX Upgrade (AUG) has contributed greatly to our understanding of the L–H transition through a combination of experimental and theoretical works. From these contributions a clearer picture of the conditions under which the L–H transition occurs has emerged and some dependencies of P_{LH} could be explained. In this paper, we present an overview of L–H transition studies at AUG. In particular the importance of the edge ion heat flux for the L–H transition and its connection to the edge radial electric field (E_r) is presented in section 2. In section 3 H-mode access in different main ion composition plasmas is discussed, while in section 4 the impact of magnetic perturbations (MPs), magnetic configuration, and wall material on P_{LH} and E_r is investigated. In section 5 we look at the I-phase and the L-mode edge turbulence and its interaction with $E \times B$ shear flows in the context of AUG experiments. In section 6 the results from AUG L–H transition studies are summarized and conclusions are drawn.

2. Connection between the H-mode power threshold, the edge ion heat flux and the edge radial electric field

One universal feature of P_{LH} is its non-monotonic dependence on the line-averaged density \bar{n}_e , (see figure 1(a)), which has been observed on many tokamaks [4, 7–12]. The H-mode power threshold exhibits a minimum at a certain plasma density, named $\bar{n}_{e,\text{min}}$. For densities both above and below $\bar{n}_{e,\text{min}}$ the power threshold increases. The parameter space below $\bar{n}_{e,\text{min}}$ is known as the low density branch, while plasmas with densities above $\bar{n}_{e,\text{min}}$ are said to be in the high density branch of the P_{LH} curve.

For the high density branch, multi-machine scalings exist [4, 5], which show an almost linear dependence on \bar{n}_e , the toroidal magnetic field B_ϕ and the plasma surface S . It should be noted that these scalings were obtained from experiments in which parameters like the plasma shape, the strike point positions, and the drift configuration were set such that P_{LH} is minimal. This was done to avoid the introduction of other dependencies, that are known to influence P_{LH} , into the scalings. Furthermore, these scalings are only correct, if the radiated power is small. As has been recently shown at AUG, in heavily seeded discharges the total radiated power up to the separatrix must be taken into account in order to reproduce P_{LH} from these scalings correctly [13]. The most commonly used scaling reads as [4]

$$P_{\text{LH,scal}} = 0.0488 \bar{n}_e^{0.717} (10^{20} \text{ m}^{-3}) B_\phi^{0.803} (\text{T}) S^{0.941} (\text{m}^2). \quad (1)$$

While the increase of P_{LH} with density and plasma size is easily understood, the magnetic field dependence is less obvious. However, this too can be understood in connection with the paradigm of edge turbulence suppression via $E \times B$ shear flows, which is described in more detail in sections 2.2 and 2.3. The multi-machine scaling, however, does not describe the behavior seen in the low density branch. A first explanation

for the increase in P_{LH} below $\bar{n}_{e,\text{min}}$, which also depends on the applied type of auxiliary heating, was extracted from experiments at AUG [14, 15] and is connected to the critical role of the edge ion heat flux ($Q_{i,\text{edge}}$). This is discussed in detail in section 2.1.

2.1. Connection between the edge ion heat flux and the low density branch

The first indication that the ion heat flux plays an important role for the L–H transition came from a set of low density AUG experiments heated with electron wave heating (ECRH) only, which enabled a decoupling of the electron and ion heat channels [14]. In these plasmas P_{LH} was measured as a function of \bar{n}_e in the low density branch. The work showed that the edge ion pressure and its gradient are important quantities at the L–H transition (see section 2.2). These observations motivated a more detailed study of the role of the ion heat channel for the L–H transition [15].

In the work of Ryter *et al* it was found that $Q_{i,\text{edge}}$ increases linearly with the plasma density across both the low- and high density branches and does not exhibit a minimum behavior, see e.g. figure 1(b), whereas the edge electron heat flux ($Q_{e,\text{edge}}$) displays a non-monotonic dependence on \bar{n}_e , similar to P_{LH} . This result was also reproduced at Alcator C-Mod where, together with the AUG data, additionally a positive B_ϕ dependence of $Q_{i,\text{edge}}$ at the L–H transition could be extracted (see equations (3) and (4) in [16]).

In the AUG data, the linear dependence of $Q_{i,\text{edge}}$ on \bar{n}_e was shown to be identical for plasmas with 0.6 and 1 MA plasma currents, despite there being almost a factor of two difference in P_{LH} between these data-sets at low density [12] (see also figure 1(b)). Note that in the high density branch, where the electron to ion heat exchange ($p_{e,i}$) is much stronger, no scaling of the power threshold with plasma current (I_p) is observed [12]. This is consistent with the lack of an I_p dependence in the multi-machine scaling for the high density branch of P_{LH} (see equation (1)). The physics behind the I_p dependence observed in the low density branch is explored further by Bilato *et al* [17]. In this work, inspired by the experimental results, Bilato *et al* developed a heuristic model for the H-mode power threshold based on the paradigm of edge turbulence suppression by $E \times B$ shear flows [18] (see also section 2.2). An important quantity in this model is the ratio of the energy equi-partition time between electrons and ions, $\tau_{e,i}$, and the energy confinement time, τ_E in L-mode [17], where the latter exhibits an almost linear dependence on I_p [19]. The model by Bilato *et al* reveals that P_{LH} depends on I_p as soon as $\tau_{e,i}$ is comparable to τ_E .

The work of Ryter *et al* demonstrated that at a given density there is a threshold in $Q_{i,\text{edge}}$ that has to be reached to trigger the L–H transition. This means a critical value of the edge ion heat flux per particle ($Q_{i,\text{edge}}/n_i$) is needed to access H-mode. The threshold value can be achieved by improving the plasma confinement, i.e. increasing τ_E , or by increasing the electron to ion heat exchange $p_{e,i}$, i.e. decreasing $\tau_{e,i}$. Since $p_{e,i} \propto n_e^2 Z_i / A_i (T_e - T_i) / T_e^{3/2}$, the electron-ion coupling can be influenced by changing the temperature ratio, e.g. with the

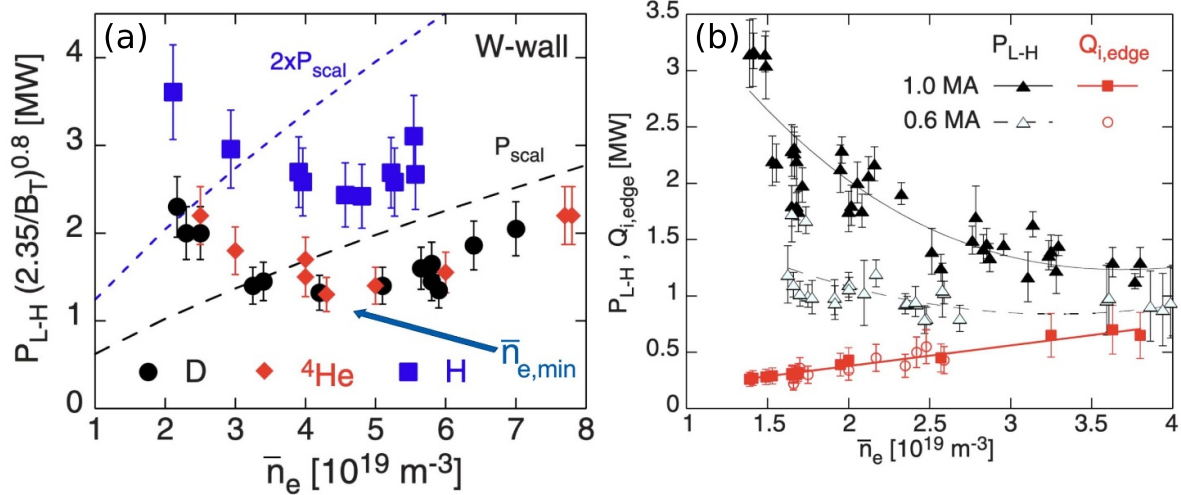


Figure 1. (a) Parabolic density dependence of the H-mode power threshold (P_{LH}) in low-torque plasmas of pure H (blue squares), D (black circles) and He (red diamonds) at AUG with full tungsten wall. The arrow indicates the density for which P_{LH} is lowest ($\bar{n}_{e,min}$). The dashed lines show the H-mode power threshold predicted by the multi-machine scaling (see equation (1)) for pure D and H plasmas, respectively, which is valid for densities higher than $\bar{n}_{e,min}$ (high density branch). Reproduced courtesy of IAEA. Figure from [12]. Copyright (2013) IAEA. (b) P_{LH} (black) and the edge ion heat flux at the L–H transition, $Q_{i,edge}$ (red) in the low density branch, demonstrating the linear dependence of $Q_{i,edge}$ with density and the plasma current dependence of P_{LH} . Reproduced courtesy of IAEA. Figure from [15]. © 2014 EURATOM.

heating method. In ECRH heated plasmas in the low density branch the power threshold is high, because a relatively large T_e/T_i is required to couple enough power into the ion channel to reach the critical $Q_{i,edge}/n_i$ needed for the L–H transition. If dominant ion heating, e.g. neutral beam injection (NBI), is used, T_i and its connected heat flux (Q_i) can be increased more easily. Thus, less heating power is needed to reach the critical $Q_{i,edge}/n_i$ and P_{LH} is reduced, as shown in [15]. This holds, however, only for low torque plasmas. If the plasma torque is not negligible, it can be seen that both the critical $Q_{i,edge}/n_i$ needed to enter H-mode and P_{LH} increase with increasing toroidal edge rotation [15, 20]. The authors of these publications speculate that this behavior can be explained by the impact of the edge rotation on the edge radial electric field. This will be discussed further in section 2.2.

Another way to improve the electron-ion coupling in the low density branch is simply to increase the plasma density. As density is increased, less applied power is required to achieve the same critical $Q_{i,edge}/n_i$ at the L–H transition. Above the density minimum, in the high density branch, the increases in the efficiency of the electron-ion coupling with increasing plasma density is small compared to the increase in the number of particles, resulting in the linear increase of P_{LH} with density. This is the reason for the minimum observed in the H-mode power threshold as a function of plasma density.

Noting that the minimum in P_{LH} as a function of \bar{n}_e is due to the collisional coupling between ions and electrons, Ryter *et al* examined the ratio of $\tau_E/\tau_{e,i}$ for several AUG discharges and found that the power threshold exhibits a local minimum when this quantity is approximately equal to 9. This result held for both the $I_p = 0.6$ and 1 MA data-sets. Based on these observations it is possible to develop a scaling for $\bar{n}_{e,min}$, which reproduces experimental results from

multiple tokamaks devices very well and provides a prediction for $\bar{n}_{e,min}$ in ITER deuterium operation with low torque input (see equation (3) in [15]). The density minimum in ITER is predicted to be $2.2 \times 10^{20} \text{ m}^{-3}$ for the half magnetic field and plasma current configuration and $4.4 \times 10^{20} \text{ m}^{-3}$ at full magnetic field and plasma current. This yields power thresholds of 16 and 41 MW for the half and full magnetic field and plasma current configurations, respectively, which should be feasible with the auxiliary heating systems planned for ITER [2].

The framework of a critical edge ion heat flux explains the minimum of the P_{LH} curve as a function of \bar{n}_e as well as the increase in the power threshold below this value. It can also unify observations made in plasmas with different heating systems, as well as with different plasma currents. However, the ion heat flux is likely not responsible for directly triggering the L–H transition. Rather, local edge quantities that are connected to $Q_{i,edge}$, such as the radial electric field (E_r) and the ion pressure gradient, are more physics-based candidates. The relationship between the surface integrated edge ion heat flux and E_r , which is a local quantity, is explored in the next section.

2.2. Connection between the edge ion heat flux and the radial electric field

One of the most commonly invoked hypotheses to explain the L–H transition is connected to the suppression of radial turbulent transport at the plasma edge by poloidally directed $E \times B$ shear flows [18]. In this framework, the condition for the H-mode access is that the $E \times B$ flow shearing rate ($\omega_{E \times B}$) is large enough to stabilize the characteristic L-mode turbulence at the plasma edge. The $E \times B$ shearing rate is given by $\omega_{E \times B} = -\frac{r}{q} \nabla_r \left(\frac{E_r}{RBq} \right)$, with q being the safety factor, r and R the

minor and major radii, respectively, and B_θ the poloidal magnetic field component [21]. Since $\omega_{E \times B}$ is directly proportional to the gradient of E_r , it is expected that E_r and its formation in L-mode are of high importance for the L–H transition.

The background radial electric field can be determined via the radial force balance

$$E_r = \frac{\nabla_r p_i}{eZ_i n_i} + v_{\perp,i} B = \frac{\nabla_r p_i}{eZ_i n_i} - v_{\theta,i} B_\phi + v_{\phi,i} B_\theta, \quad (2)$$

where p , n , and v represent the pressure, density, and flow velocity of any plasma species and eZ its charge. B is the total magnetic field and B_θ and B_ϕ its poloidal and toroidal components, respectively. The flow perpendicular to the magnetic field, $v_{\perp,i}$, can also be decomposed in its toroidal and poloidal components $v_{\phi,i}$ and $v_{\theta,i}$. Although the formula holds for all plasma species (E_r must be the same for all plasma species), the behavior of the main ion species, denoted with i here, is of particular interest for the formation of E_r .

Assuming that the poloidal main ion rotation is determined by neoclassical theory and that the toroidal main ion rotation is small, the radial electric field can be expressed in the following form [22, 23]

$$E_r = E_{r,\text{neo}} = -\frac{T_i}{eZ_i} \left(\frac{1 - K_1}{L_{T_i}} + \frac{1}{L_{n_i}} \right), \quad (3)$$

where the diamagnetic pressure gradient term $(\nabla_r p_i)/(Z_i e n_i)$ was re-written in terms of the logarithmic radial gradients of main ion temperature $1/L_{T_i}$ and density $1/L_{n_i}$, with $1/L_x = -\frac{\nabla_x x}{x}$. K_1 is the neoclassical flow coefficient, which depends on collisionality [23–25].

At typical AUG edge parameters the ion collisionality is in the plateau-regime [26–28] and $K_1 \approx 0$. Thus, $E_r \approx (\nabla_r p_i)/(Z_i e n_i)$ or $|v_{E \times B}| \approx |v_{\text{dia},i}|$, which is called the neoclassical approximation in the following. It has been found in AUG H-modes that E_r can be indeed approximated in this form [29], but in L-modes it is also often observed that E_r deviates from $E_{r,\text{neo}}$ as well as that the toroidal rotation is not small and, thus, $v_{\phi,i} B_\theta$ is a non-negligible contribution to E_r (see sections 2.3 and 4.3).

One possible interpretation within the paradigm of turbulence suppression by background $E \times B$ shear flows is that externally controllable quantities like density and heating power lead to a steepening of the background edge gradients in L-mode, which impact the E_r gradients and their related $E \times B$ shear flows mainly via $(\nabla_r p_i)/(Z_i e n_i)$. At the plasma edge E_r typically develops a well-like structure with two gradients of opposite sign. However, it is unclear if the negative (inner) or the positive (outer) gradient is of more importance for the transition into H-mode. Therefore, in this article it is not separated between the two gradients and their connected $E \times B$ shear layers, as either of them could be important for the H-mode access, although experiments at AUG indicate that the edge turbulence suppression starts at the location of the inner shear layer [30]. In this framework, H-mode is then achieved as soon as a ‘threshold’ value in $\omega_{E \times B}$ is reached,

i.e. one that is large enough to suppress the turbulent transport in the edge. At AUG it has been found that, when moving from L-mode towards the L–H transition it is mainly $1/L_{T_i}$ which changes, while the density gradient contribution, approximated by $1/L_{n_e}$, stays fairly constant [31, 32]. However, if by any means, e.g. wall condition, the latter is changed, then this also has an impact on the required power needed to enter H-mode, as will be shown in section 4.1.

These observations on local parameters at the plasma edge are in line with the findings of the critical role of $Q_{i,\text{edge}}$ at the L–H transition, discussed earlier in section 2.1. Although within the paradigm of turbulence suppression by $E \times B$ shear flows, it is not $Q_{i,\text{edge}}$ itself that is expected to be important, but rather ∇E_r and $\omega_{E \times B}$, these quantities are all related to the main ion temperature gradient: E_r via equation (2) and the edge ion heat flux via $Q_{i,\text{edge}} = -\chi_i n_i \nabla T_i$, with χ_i being the ion heat diffusivity. Within this picture, the increase in P_{LH} and the required $Q_{i,\text{edge}}$ to initiate an L–H transition observed in higher rotation plasmas can also be explained. If the increased rotation reduces the local $E \times B$ shear, a higher applied heating power (and $Q_{i,\text{edge}}$) would be required to further increase the edge ion temperature gradient, compensating for the impact of the rotation, to obtain the same edge E_r .

The interconnections between $Q_{i,\text{edge}}$ and E_r , as they relate to P_{LH} , were already pointed out in [14], where detailed analysis of the edge kinetic profiles demonstrated that the edge electron temperature $T_{e,\text{edge}}$ increases linearly with applied ECRH power at constant plasma density, whereas $T_{i,\text{edge}}$ remains fairly constant. The same observations were also made in H plasmas in [33]. As a result, the ion pressure at the plasma edge ($p_{i,\text{edge}}$) was observed to increase linearly with increasing plasma density at the L–H transition, as did $Q_{i,\text{edge}}$, whereas $p_{e,\text{edge}}$ behaves more like $Q_{e,\text{edge}}$ and P_{LH} at the L–H transition.

In the work of Sauter *et al* it was also found that the minimum of the E_r well, $E_{r,\text{min}}$ is constant at the L–H transition ($E_{r,\text{min}} \approx -15 \text{ kV m}^{-1}$) for plasmas with a constant magnetic field of -2.5 T , but different densities (covering the low and high density branch of P_{LH}). In that work the edge radial electric field was to a large extent not directly measured, but deduced from edge temperature and density measurements together with neoclassical theory using equation (3). Assuming now additionally that the width of the E_r well is constant, as was found experimentally in H-modes at AUG [34], then the value of the E_r minimum can be used as a proxy for its gradients. In conclusion, the work of Sauter *et al* shows experimentally, that for a wide range of plasma densities the E_r gradients are constant at the L–H transition. Similar assumptions on the edge E_r in L-mode plasmas were made by Maggi *et al* on JET data [35]. In this work the same conclusions for JET L–H transitions were drawn as previously for AUG, where they showed that an apparent threshold in the minimum value of E_r is required to enter H-mode.

It should be noted that all the experiments described so far were carried out for a fixed magnetic field value and in a single magnetic field configuration, namely lower single null,

favorable drift. The impact of changes in these two parameters are described in the following section and in section 4.3, respectively.

2.3. Magnetic field dependence of the H-mode power threshold

Building on the L–H transition results described in the previous sections, the relationship between the actual measured edge E_r and P_{LH} was investigated further by Cavedon *et al* [36] by exploring the magnetic field dependence of P_{LH} (see equation (1)) in deuterium (D) and a small subset of hydrogen (H) discharges. In this work the L-mode edge E_r prior to the L–H transition was measured with 1–2 ms time resolution using a fast charge exchange recombination spectroscopy (CXRS) technique [37]. Due to the limited radial resolution of this method, it was not possible to extract meaningful E_r gradients from the experimental data directly. Therefore, again $E_{r,\text{min}}$ was used as a proxy for the E_r gradients (see also section 2.2). It was observed that $E_{r,\text{min}}$ at the L–H transition deepens linearly with increasing magnetic field. This results in an almost constant $E \times B$ velocity shear at the L–H transition, since $\omega_{E \times B} \propto \nabla_r \frac{E_r}{B} \propto \left| \frac{E_{r,\text{min}}}{B} \right| = \max(|v_{E \times B}|)$. This observation is an important result to distinguish experimentally $v_{E \times B}$ as a more fundamental quantity for the L–H transition than E_r .

The work by Cavedon *et al* also showed that the maximum in $|v_{E \times B}|$ at the L–H transition remains constant as a function of electron density for the different magnetic fields explored and that this value is consistent with earlier data-sets [14, 26]. This is shown in figure 2(b). Here, the maximum of the measured $|v_{E \times B}|$ is shown for the entire data-set from the work by Cavedon *et al* (circles and squares) and is compared to the results from the previous works (diamonds and triangles), neither of which directly measure E_r (or $v_{E \times B}$), but used the neoclassical approximation $|v_{E \times B}| = |v_{\text{dia},i}|$. Combining all the data-sets, a threshold value of $|v_{E \times B}| = 6.7 \pm 1.0 \text{ km s}^{-1}$ was found at the L–H transition. Since in these data-sets P_{LH} varied by a factor of about three, this result provides a clear, concise explanation for the observed dependence of P_{LH} on B_ϕ (see equation (1)). A critical threshold in $v_{E \times B}$ needed to enter H-mode automatically incorporates the observed magnetic field dependence, as has also been shown with fluid codes modelling the L–H transition (see [38] and references therein). Increasing the magnetic field reduces $v_{E \times B}$ such that steeper E_r gradients are required and, hence, a higher edge ion pressure gradient, edge ion heat flux, and P_{LH} , in order to obtain the same critical $v_{E \times B}$ shear at the L–H transition. It is important to note that the same value for the critical $v_{E \times B}$ was found in both H and D plasmas. This has important ramifications for interpretation of differences seen in P_{LH} between different hydrogen isotopes and will be discussed further in section 3.

It is worth mentioning that the work by Cavedon *et al* examined the scaling of $E_{r,\text{min}}$ with magnetic field in the high density branch only. However, together with the previously reported results on the critical role of E_r and $Q_{i,\text{edge}}$ in the low

density branch [14, 15], it is likely that the magnetic field scaling of $E_{r,\text{min}}$ seen by Cavedon *et al* would also be recovered in the low density branch. As such, $v_{E \times B}$ seems to be a more fundamental quantity for the L–H transition than E_r itself, and this observation is consistent with the magnetic field scaling of $Q_{i,\text{edge}}$ at the L–H transition found in Alcator C-Mod [16], which is valid for all plasma densities.

At AUG the experimental investigations into the role of the radial electric field and its associated quantities in the L–H transition has continued with ever improving diagnostic capabilities and expanding the explored parameter space. Recent experiments pushed to even lower densities [27, 32]. It is interesting to compare the minimum of $v_{E \times B}$ from these new measurements with the previous data-sets presented in [36]. This comparison is shown in figure 3.

The new measurements of $v_{E \times B}$ at the L–H transition, determined with He II spectroscopy (HES) [32] and Doppler reflectometry (DR), are shown as blue circles for D and red squares for H plasmas in figure 3. As shown in [32], the two E_r measurement techniques exhibit excellent agreement in L-mode plasmas. This new data-set contains data from plasmas heated with ECRH only, with a constant magnetic field of -2.5 T at the geometric axis, and a plasma current of either 0.8 or 1.2 MA. For the entire covered density range, no difference in the minimum of $v_{E \times B}$ is found between H and D plasmas, which is consistent with former observations at AUG [36], and between the low and high plasma current discharges. The latter is consistent with the findings by Ryter *et al* that $Q_{i,\text{edge}}$ at the L–H transition does not show any dependence on I_p (see also section 2.1).

For comparison of the new data with the old data-sets, the $v_{E \times B}$ data points from Cavedon *et al*, measured with CXRS, are shown in figure 3 as grey points, while the data points from [14, 26], for which the neoclassical approximation was applied to determine E_r , are plotted in black. Above an edge density of $2.5 \times 10^{19} \text{ m}^{-3}$ a direct comparison between the different measurement techniques is possible. There is good agreement between the results within error bars, although the new measurements give a systematically lower $\max(|v_{E \times B}|)$ than the old ones. Below an edge density of $2.5 \times 10^{19} \text{ m}^{-3}$, which corresponds to a plasma located in the low density branch of P_{LH} , a clearly lower critical $v_{E \times B}$ is measured than is expected from the approximation $|v_{E \times B}| \approx |v_{\text{dia},i}|$. This deviation indicates not necessarily that the poloidal rotation is non-neoclassical, but that under these plasma conditions, i.e. at low density, the toroidal main ion flow is not negligible and has to be taken into account in the determination of E_r , as also shown in [27].

The variation in the measured $\max(|v_{E \times B}|)$ at the L–H transition does also not necessarily imply that the shear of $v_{E \times B}$ is not constant at the L–H transition. As it is regularly observed in ECRH heated plasmas, in which the toroidal main ion flow is purely intrinsic, the latter just leads to a shift of the entire edge $v_{E \times B}$ profile, leaving its gradients nearly unchanged, but reduces $\max(|v_{E \times B}|)$ [27, 39]. This implies that the same criterion for turbulence suppression by a critical $\omega_{E \times B}$ can still hold, as discussed later in section 4.2, but

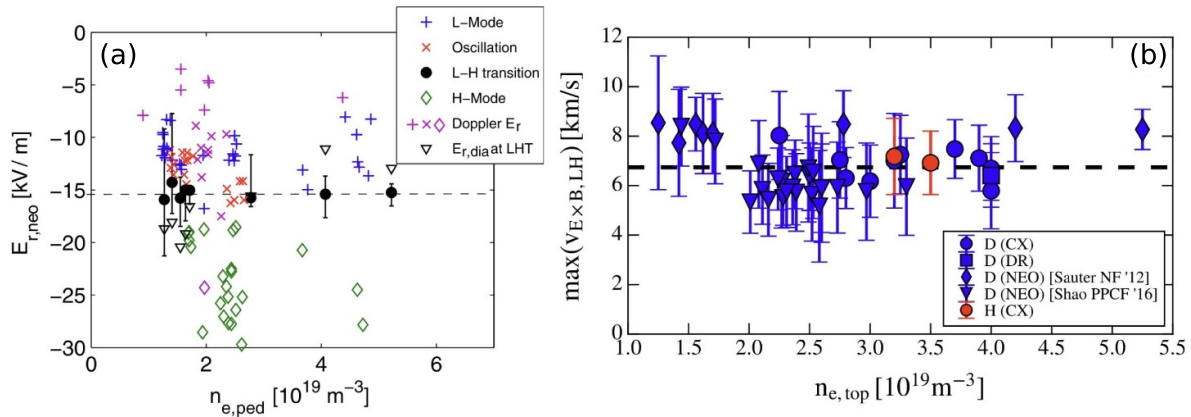


Figure 2. (a) Neoclassical approximation ($E_{r,neo}$) and Doppler reflectometry (DR) measurements (purple) of the minimum of the radial electric field well at the plasma edge in a range of plasma confinement states. At the L–H transition (black circles) a value of $E_{r,neo} \approx -15 \text{ kV m}^{-1}$ is found at AUG for a wide range of edge densities in favorable drift plasmas with $|B_\phi| = 2.5 \text{ T}$. Reproduced courtesy of IAEA. Figure from [14]. Copyright (2012) IAEA. (b) Maximum of $|v_{E \times B}|$ at the L–H transition plotted against plasma edge density ($\rho_{pol} \approx 0.95$) for a range of favorable drift plasma discharges in which also $|B_\phi|$ was varied from 1.7 to 3.0 T. The figure includes the points at the L–H transition from (a) (diamonds) as well as actual measurements of the $v_{E \times B}$ minimum by CXRS (circles) and DR (squares). Red points are $v_{E \times B}$ measurements acquired in hydrogen and blue points are from deuterium plasmas. Reproduced courtesy of IAEA. Figure from [36]. © EURATOM 2020.

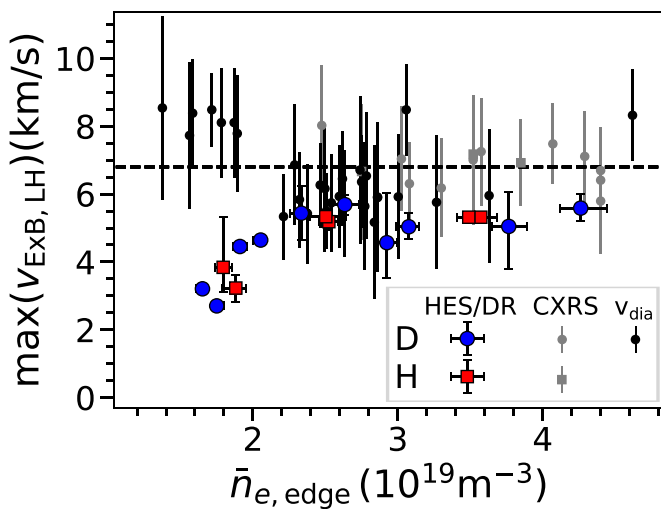


Figure 3. Minimum of the experimentally determined edge $v_{E \times B}$ at the L–H transition plotted against the plasma edge density. The measurements were made with He II spectroscopy (HES) [32] and Doppler reflectometry (DR) in D (blue circles) and H (red squares) plasmas of favorable drift configuration with $B_\phi = -2.5 \text{ T}$ and $I_p = 0.8$ or 1.2 MA . The data of figure 2 are also plotted in this figure for comparison. Here, the experimental data acquired with CXRS [36] are shown as grey symbols, while the data of [14, 26], using the neoclassical approximation $|v_{E \times B}| \approx |v_{dia,i}|$, are shown as black symbols.

the assumption that the minimum of E_r is a proxy for its gradients is not valid under these conditions. A quantitative assessment of the E_r gradients and their related $E \times B$ shearing rates is foreseen for this new data-set, which will require a systematic and careful study of the radial uncertainties of the measured E_r profiles. It should also be noted that recent work by Silva *et al* [40] shows E_r measurements at the L–H transition

in the JET tokamak and reports on very similar observations as presented here for AUG.

In summary, the framework of a critical $Q_{i,edge}$ is able to explain the experimental observations in the low density branch of the P_{LH} curve and the density minimum. It is also able to unify experimental observations of P_{LH} in this parameter regime for plasmas with different combinations of ion and electron heating, making $Q_{i,edge}$ a more physical macroscopic quantity for understanding L–H transitions than P_{LH} . However, $Q_{i,edge}$ alone is not able to explain all of the experimental observations, for example, the dependence on the magnetic field is only explained by connecting $Q_{i,edge}$ to $v_{E \times B}$ and its shear. In addition, $Q_{i,edge}$ does not provide a direct explanation for the dependence of P_{LH} on the main ion species or on the magnetic configuration. Instead, to understand these phenomena, local edge quantities, like E_r , have to be investigated and linked to the characteristics of the edge turbulence.

3. Impact of main ion species composition on the L–H transition

A dependence of P_{LH} on the main ion plasma species was found already in early isotope experiments [41, 42]. For hydrogenic species P_{LH} scales with the inverse of the main ion mass A_i . Thus, in hydrogen (H) plasmas P_{LH} is about two times larger than in deuterium (D) plasmas [42]. The H-mode power threshold for pure helium (He) plasmas varies for different machines between 1 and $1.8 \times P_{LH}(D)$ [20, 41]. In the past years, more experimental and theoretical investigations have been performed at AUG to elucidate the reasons for the dependence of P_{LH} on the main ion species. The most important results of these investigations in pure D, H and He plasmas and in mixed H–He and H–D plasmas are presented in the following.

3.1. Pure H, D and He plasmas

Figure 1(a) shows the parabolic dependence of the H-mode power threshold on electron density as measured in AUG pure H, D and He plasmas. The corresponding experiments were all performed after the switch from a carbon to a tungsten wall [12] and the identification of the power threshold at low density was made possible by the extension of the ECRH systems on AUG [43]. The data show that in a metal-wall AUG $P_{\text{LH}}(\text{He}) \approx P_{\text{LH}}(\text{D})$ [44]. Recent measurements in He plasmas at AUG could confirm this result [32], which is different from observations in carbon wall machines, where it is found that P_{LH} in He is higher than in D by about 40% [10, 44, 45]. The latter is also the current assumption for ITER He operation, namely that $P_{\text{LH}}(\text{He}) \approx 1.4 \times P_{\text{LH}}(\text{D})$ [2]. However, recent experiments at JET have also found comparable power thresholds between helium and deuterium with the ITER-like wall when considering the high density branch [46]. On the other hand, the density minimum is shifted towards higher values for He in JET, implying that $P_{\text{LH}}(\text{He}) > P_{\text{LH}}(\text{D})$ at the respective density minimum, which is not observed at AUG. At AUG the density minimum and P_{LH} at the density minimum are the same in He as in D plasmas [12].

As can be seen in figure 1(a), also in the all metal-wall AUG P_{LH} is twice as high in pure H compared to pure D plasmas. Therefore, the role of the edge ion heat flux at the L–H transition was investigated also in pure H plasmas [33] and it was found that $Q_{i,\text{edge}}$ is as well twice as large in H as it is in D, but again it increases linearly with the plasma density. Although this means that there is not one critical value of $Q_{i,\text{edge}}/n_i$ at the L–H transition, which unifies observations in deuterium and hydrogen plasmas, it is also known that the turbulent transport is increased in H compared to D plasmas (see [47] and references therein). In the framework of a critical $E \times B$ shear needed to trigger the L–H transition, this would imply that, due to the increased turbulent transport, more heating power is needed in H plasmas to establish the same critical edge gradients required at the L–H transition. This, in turn, results in a higher P_{LH} and a higher $Q_{i,\text{edge}}$ for H plasmas. On the other hand, one might also expect that the higher turbulent transport level in H would require a higher $E \times B$ velocity shear at the L–H transition to be able to suppress the characteristic edge turbulence.

In several comparative experiments, the edge E_r or its minimum were measured at the L–H transition in both D and H plasmas at AUG. As can already be seen from figures 2(b) and 3, the minimum of $v_{E \times B}$ at the L–H transition is the same in D and H for a given plasma density (see section 2.3 for a description of the different data-sets). More recent E_r measurements with improved diagnostic capabilities (HES and DR) [32] show that not only the minimum of E_r is the same for D and H plasmas at the L–H transition, but also the width of the E_r well is of comparable size. This is shown in figure 4 and justifies that in these conditions, i.e. the high density branch, $E_{r,\text{min}}$ can be used as a proxy for its gradients. It is also observed that for some plasma conditions, i.e. same plasma density and same heating method, the strength of both the inner

and the outer E_r gradient are the same between D and H, despite a factor of 2–3 difference in the amount of applied heating power (see also figure 4). Further analysis of the edge profiles has revealed that also the edge ion pressure gradient is comparable in D and H plasmas at the L–H transition [33, 48]. These experimental results confirm the hypothesis that in hydrogen plasmas a higher applied power (and edge ion heat flux) is required to obtain the same critical edge gradients at the L–H transition as seen in deuterium, on account of the higher ion heat transport. Hence, the same conditions as observed in D plasmas seem to hold quite robustly also in H, when the differences in the turbulent heat transport as a function of ion mass are taken into account. It should be noted that similar observations have also been made by Birkenmeier *et al* in recent isotope L–H transition experiments at JET [49, 50].

Several recent theoretical works studying the turbulence in the L-mode edge have identified collisional drift-wave turbulence as the dominating transport mechanism [51–53], due to the increased collisionality in that region. This is in contrast to the ion-temperature-gradient/trapped-electron-mode instabilities typically present in the plasma core. The presence of drift-waves makes the parallel electron dynamics in the gyrokinetic equation important for simulating the transport and the ion mass dependence enters via the electron to ion mass ratio important for the electron dynamics. As can be seen in figure 9 of [51], at high collisionality the turbulence growth-rates are expected to be a factor of two larger in H compared to D.

Within the framework of turbulence suppression by the background $E \times B$ shear as the mechanism initiating the L–H transition, one would expect that a corresponding increase in $\omega_{E \times B}$ would be required in hydrogen to enter H-mode, in seeming contradiction with the experimental data. In the work of Cavedon *et al* [36], as well as the newest results presented here (see figures 3 and 4), no difference in $v_{E \times B}$ (or E_r) at the L–H transition are observed between hydrogen and deuterium. The lack of difference is potentially explained within the simulations, at least in part, by the highly non-linear response of the plasma turbulence to the $E \times B$ shear as well as the inter-dependencies with other plasma parameters [31, 54]. Bonanomi *et al* showed that at low plasma β the inclusion of the $E \times B$ shear in the simulations has only a small impact on the turbulence, while at higher β the effect is non-linear, with small increases in $\omega_{E \times B}$ resulting in strong turbulence suppression [31, 54]. This effect is tied to the type and scale of the turbulent structures, with larger scale (low k_y) instabilities being found when increasing the edge plasma β . The simulations highlight the differences expected in the turbulence properties between hydrogen and deuterium plasmas, but also as a function of plasma β . In both deuterium and hydrogen plasmas β changes in response to multiple design parameters including magnetic field, plasma current, electron density and applied heating power. As such, all of these changes are expected to also impact the turbulence properties at the edge, making the constant $v_{E \times B}$ value found over a wide range of parameters in deuterium just as unexpected as finding the same value present in both H and D plasmas.

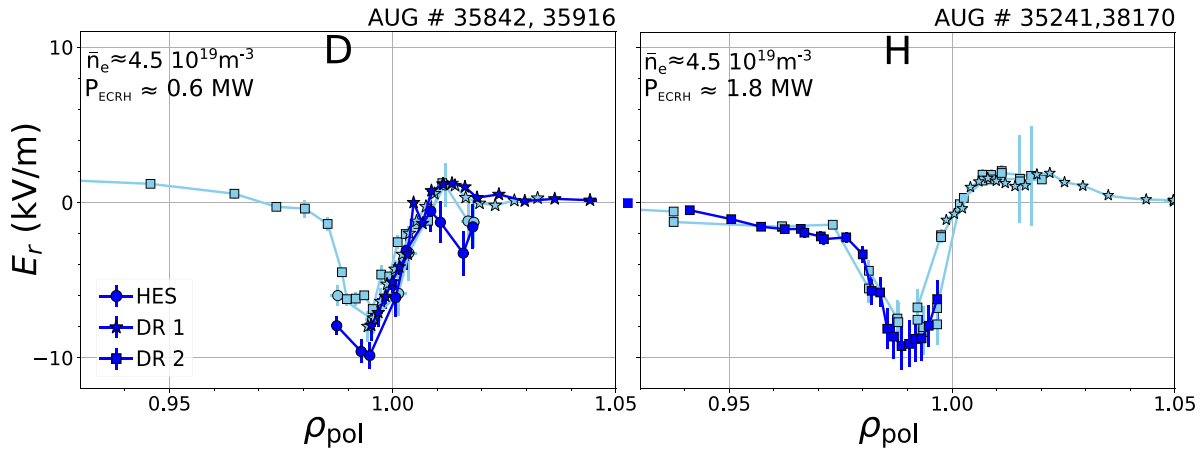


Figure 4. Experimental measurements, acquired with He II spectroscopy (HES) and Doppler reflectometry (DR), of E_r profiles at the L–H transition in pure deuterium plasmas (left) and pure hydrogen plasmas (right). They reveal that the edge E_r , including its gradients, is very similar for the two ion species at the respective confinement transition.

The AUG results, in combination with the new simulations, suggest the following qualitative picture: In a given L-mode plasma, the application of external heating increases the power in the ion channel and, thus, the edge ion heat flux, the edge ion temperature gradient and the gradients in the radial electric field as well as the $E \times B$ shear. At the same time, the increase in applied power increases the plasma pressure, altering the turbulence structures at the edge towards larger scale instabilities that are strongly, and non-linearly susceptible to $E \times B$ shear stabilization. The strongly non-linear turbulence suppression as a function of increasing $\omega_{E \times B}$ is qualitatively and to some extent quantitatively consistent with the experimental data [31, 54]. From a purely experimental perspective the data demonstrate a clear $v_{E \times B}$ threshold for the L–H transition, which applies equally well to both D and H plasmas. The observed increase in P_{LH} in H compared to D directly follows from this result, when combined with the well understood changes in the edge turbulent transport.

3.2. Mixed H–D and H–He plasmas

It is also of interest to examine how P_{LH} changes when transitioning from one main working gas to another and in plasmas with mixed main ion species. The latter is particularly relevant for reactors that will operate with 50–50 D–T mixtures, while the former is of interest for the start-up phase of ITER operation [2]. The power threshold in D–T plasmas has recently been investigated in JET [49, 55], while experiments at AUG have focused on the behavior of P_{LH} in hydrogen–deuterium mixes as well as hydrogen plasmas seeded with controlled amounts of He [56]. The latter experiments were motivated by observations at JET that showed a strong reduction of P_{LH} in NBI heated H plasmas with modest levels of He seeding (He concentration $c_{He} = n_{He}/n_e$ up to 10%) [57]. As discussed in the previous section, in AUG the power threshold in H is twice as large as in D, while in He it is similar to the deuterium threshold. Hence, during the transition from a hydrogen-dominated plasma to a He plasma, it is reasonable to expect a decrease in P_{LH} from the H to the He level.

This transition was explored in AUG experiments in which H plasmas were seeded with controlled amounts of He up to a He concentration of 20% [56]. The obtained P_{LH} values, also normalized by the multi-machine scaling of D plasmas (see equation (1)) to account for the slight density increase with increasing amount of He seeding, are shown in figures 5(a) and (b), respectively. No change in the threshold is observed, inconsistent with the JET observations [57], but consistent with previous AUG results, where a reduction in P_{LH} when moving from H to He was only obtained at c_{He} values of about 30% [44]. Note that at $c_{He} = 20\%$, with the typically low-Z impurity levels at AUG, the H concentration is still more than 50% of the electron density. However, at 30% He concentration $n_{He}/n_H > 1$, making it effectively a He plasma with hydrogen seeding.

The AUG P_{LH} results were all obtained in plasmas close to the density minimum. Thus, they are consistent with recent DIII-D results [58], which also show no change in the high P_{LH} of hydrogen at low He seeding levels ($c_{He} < 20\%$) for plasmas located in the high density branch. The very strong reduction of the hydrogen power threshold by about 25% for less than 10% He seeding as observed at JET is, therefore, not reproduced by either the AUG or the DIII-D experiments.

In contrast to JET, most of the plasmas in the AUG experiments were heated with ECRH (blue circles in figure 5), also NBI heating was used for a small subset of discharges (red squares). As can be seen in figure 5, P_{LH} in the NBI heated plasmas is by about 20% higher than in the ECRH cases. As discussed previously in section 2, at several tokamaks such a difference in P_{LH} between NBI and ECRH heated plasmas is observed, which is related to the differences in torque input and toroidal edge rotation and its effect on E_r . For the here presented H plasmas with He seeding the change in edge rotation alone was, however, not big enough to explain the differences in P_{LH} [56]. Another effect was at play, which was resolved via power balance calculations. They show that at the L–H transition $Q_{i,edge}$ is the same within the uncertainties for both the ECRH and the NBI heated plasmas and that this value remains constant over the entire range of explored He seeding

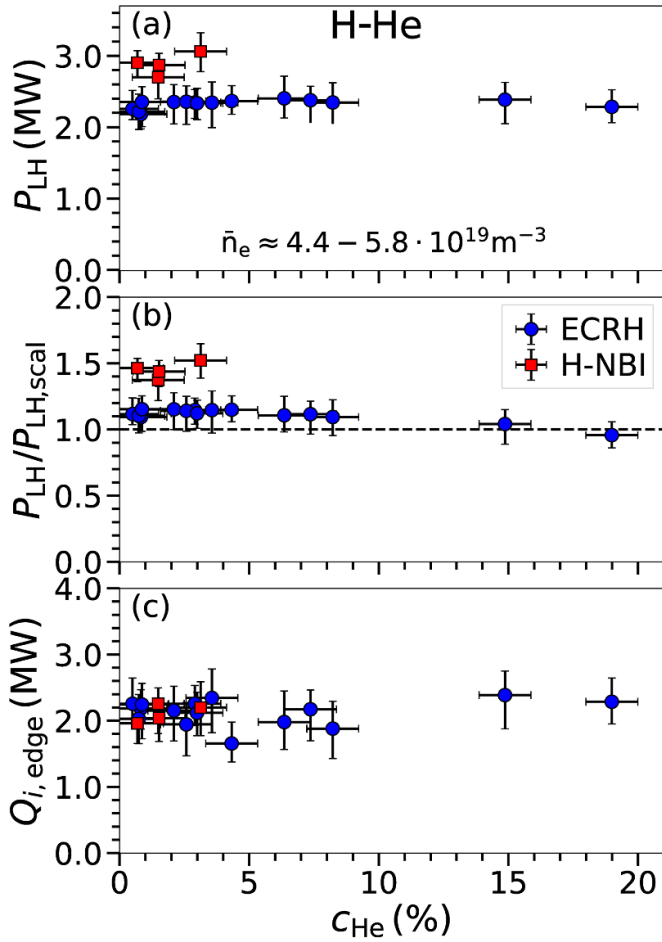


Figure 5. (a) H-mode power threshold in NBI (red) and ECRH (blue) heated mixed hydrogen–helium plasmas plotted against the He concentration (in % of the electron density). The high P_{LH} in H plasmas does not decrease significantly with admixture of up to 20% of He, even if the density increase due to the additional He injection is taken into account, by normalizing P_{LH} to the multi-machine scaling [4] (b). The edge ion heat flux at the L–H transition (c) is also found to be the same independent of the He concentration and external heating source. Reproduced courtesy of IAEA. Figure from [56]. © EURATOM 2020.

levels, see figure 5(c). The differences observed in P_{LH} with heating method are related to the higher impact of the heat exchange term ($p_{e,i}$) on $Q_{i,edge}$ in H plasmas compared to D plasmas (inverse mass dependence, see section 2.1) and the dependence of $p_{e,i}$ on the temperature ratio T_e/T_i , which is actively influenced by the heating method. While in ECRH heated plasmas T_e/T_i is larger, increasing $p_{e,i}$ and, thus, $Q_{i,edge}$ in L-mode plasmas at the density minimum, in NBI plasmas this ratio is smaller, requiring more heating power to reach the critical $Q_{i,edge}$ needed to enter H-mode [56].

The results from these L–H experiments in mixed H–He plasmas conducted at AUG also show that in plasmas in which the heat exchange term is the dominant contribution to $Q_{i,edge}$, the H-mode access is determined by the transport properties of the plasma core. This will also be the case in ITER PFPO-1 in which only ECRH is available [2].

At AUG the behavior of P_{LH} across the transition from deuterium to hydrogen dominated plasmas has also been

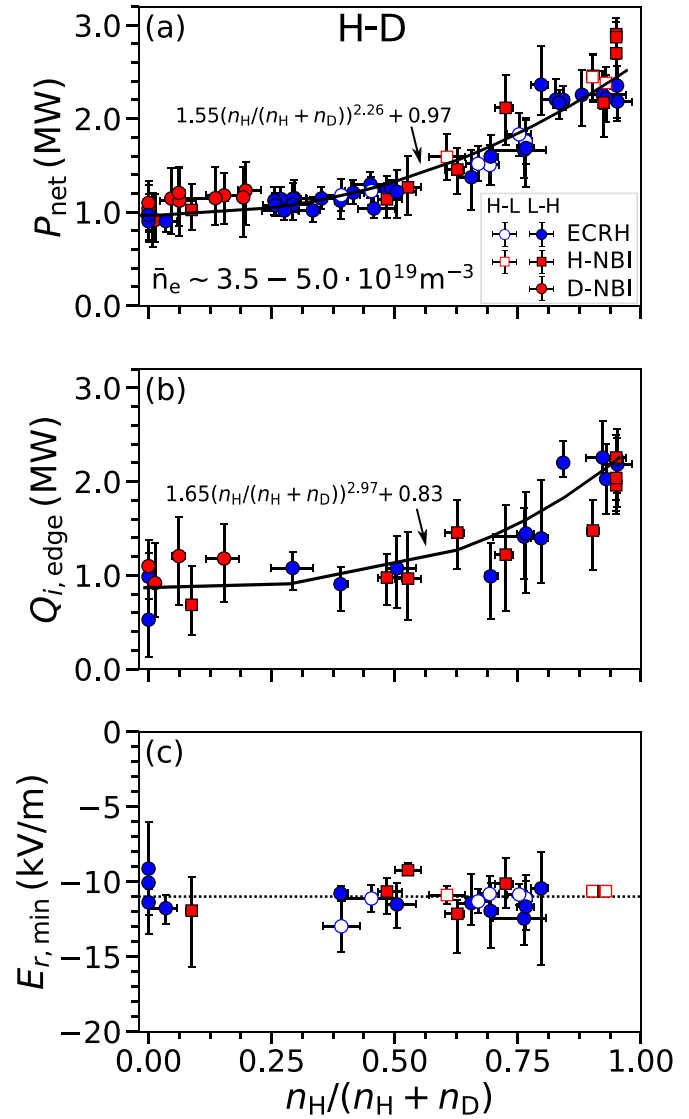


Figure 6. (a) Net input power at the L–H transition (colored symbols) and the H–L back transition (white symbols) plotted against the relative hydrogen content. Both P_{LH} and P_{HL} increase non-linearly with increasing hydrogen content, which is also indicated by the black line, a fit to the experimental data. (b) The edge ion heat flux at the L–H transition exhibits a similar increase with relative hydrogen content as P_{LH} . (c) The minimum of E_r , which can be used as a proxy for its gradients at these plasma densities, is constant at about -11 kV m^{-1} , independent of the hydrogen content and for both the L–H and the H–L back transition.

investigated and results from the initial experiments were presented in [56]. Since then, the investigations have been expanded to cover the complete transition from hydrogen to deuterium, see figure 6, which combines the originally published data-set with the new results. P_{LH} and $Q_{i,edge}$ exhibit a very similar dependence on the relative hydrogen content ($n_H/(n_H + n_D)$), with both remaining at the deuterium level until the plasma is about 50% H, as reported in [56]. Between $n_H/(n_H + n_D) = 0.5$ and 1 both quantities start to increase, which is shown in figure 6(a) for P_{LH} and in figure 6(b) for $Q_{i,edge}$. This results in a non-linear increase of P_{LH} and $Q_{i,edge}$ with $n_H/(n_H + n_D)$, as indicated by the respective fit functions in the figure (black solid lines).

Besides the L–H transition, also the H–L back transition was investigated in these mixed H–D plasmas. While colored symbols correspond to the L–H transition in figure 6, the H–L back transition is depicted with the white symbols. P_{HL} aligns very well with P_{LH} , but the lack of hysteresis, which is usually observed [12], can be ascribed to the fact that the density dependence is not captured in figure 6(a). Due to the design of the discharges, the L–H transitions occur systematically at lower plasma densities than the respective H–L back transitions. If the density increase were taken into account, a hysteresis between P_{LH} and P_{HL} would be visible.

Figure 6(c) shows the minimum of the radial electric field measured at these various transitions. Consistent with previous data-sets in pure D and H plasmas (see section 3.1), $E_{r,\min}$ is found to remain constant at about -11 kV m^{-1} regardless of the main ion species mix. As $E_{r,\min}$ can be used as a proxy for its gradients in these plasma conditions (see sections 2.3 and 3.1), this observation implies that the $v_{E \times B}$ shear must be constant, independent of the main ion species composition. The constant $E \times B$ shear together with the non-linear increase of P_{LH} and $Q_{i,\text{edge}}$ with increasing $n_H/(n_H + n_D)$ indicates, according to previous argumentation (see section 3.1), that also the L-mode edge turbulent transport increases non-linearly with increasing hydrogen content. It is foreseen to reproduce this observed dependence of the L–H transition on the effective main ion mass in gyrokinetic simulations and a semi-analytical model developed for the L–H transition at AUG (see section 5.1).

Also $E_{r,\min}$ does not show any hysteresis and has the same value of about -11 kV m^{-1} at the L–H as well as at the H–L back transition. This is consistent with previous measurements of the electron pressure gradient at the L–H and H–L back transition. For medium plasma densities, where electrons and ions are coupled, it was found that the H–L back-transition occurs at the same electron pressure gradients as the L–H transition [59]. The experimentally observed lack of hysteresis in local edge quantities compared to macroscopic quantities, like the power threshold, is quite interesting, as it suggests that, despite different edge transport properties in H- and L-mode, at the L–H transition the same criterion must hold which leads to the confinement transition. This reinforces the need for self-consistent simulations of edge turbulence-flow interaction in order to reproduce an entire L–H–L cycle correctly.

4. Impact of magnetic configuration and wall condition on the H-mode power threshold

In section 2 a relatively simple explanation for the B_ϕ dependence of P_{LH} was presented. However, not only the magnetic field strength, but also the magnetic field geometry can influence P_{LH} . A very well known example of this is the observation that P_{LH} is different by roughly a factor of two depending on the direction of the ion $\nabla B \times B$ drift relative to the active X-point of single-null magnetic configurations. When the ion $\nabla B \times B$ drift points towards the active X-point P_{LH} is lower than when the ion $\nabla B \times B$ drift points away from the active

X-point. Hence, it is the practice to refer to the former configuration as ‘favorable’ and to the latter as ‘unfavorable’. This observed difference in P_{LH} with drift configuration, despite being well known for many years, does not have a robust explanation. Recent AUG experiments, aimed at illuminating this dependence of P_{LH} [27], are presented in section 4.3.

In addition to the X-point configuration, perturbations to the magnetic field, such as those imposed for suppression of edge localized modes (ELMs), have also been observed to impact the H-mode power threshold [10, 60–66]. ITER plans to use MP coils to achieve the desired ELM suppression and ideally to apply them before the L–H transition, such that even the first ELM can be avoided. As such, any changes to the power threshold in the presence of MPs is very relevant for ITER operation. For this reason experiments to explore this issue were performed at AUG [39]. The results of these experiments are summarized in section 4.2.

These examples demonstrate that changes in the plasma edge and the scrape-off layer (SOL), either due to drifts, details of the magnetic geometry, or SOL transport can influence the confined region and P_{LH} . Another example of this is the influence of the wall material on the H-mode power threshold. While not intuitive, the impact of wall material on P_{LH} , specifically the reduction seen in metal-walled devices compared to carbon-walled machines, is a robust observation, first seen at AUG [12], and discussed in detail in section 4.1.

4.1. Wall material

AUG’s gradual transition from a carbon (C) wall to a pure tungsten (W) wall provided an unprecedented opportunity to study the impact of wall material on tokamak operation, including plasma confinement, density and impurity control, pedestal transport, and the L–H transition. The wall material transition took place gradually between 2003 and 2007 [67], at which time also a cleaning of the machine was performed to remove the residual carbon from the tungsten surfaces. In 2007 and 2008 two full AUG operational campaigns were dedicated to exploring tokamak operation in the absence of low-Z wall materials. Therefore, no boronizations or other low-Z wall coating methods were employed during this time. A robust observation from these campaigns, and all subsequent campaigns in AUG with W wall, is a reduction of the H-mode power threshold by 25% compared to the C wall [12]. A similar 30% reduction of P_{LH} was then also observed at JET after the transition to the ITER-like wall [35].

The similarity of observations between the two machines provides additional confirmation of the ubiquity of this result, which has important ramifications for ITER. Due to its metal wall, the H-mode power threshold in ITER in D is expected to be lower than P_{LH} predicted by the multi-machine scaling [4]. In addition, the power threshold in hydrogen plasmas was also explored, and a similar reduction of the power threshold between the C and W wall was observed [12, 56]. As such, this effect is expected to also apply to the early non-nuclear phases of ITER operation.

The reduction of P_{LH} with a metal wall is not due to increased and unaccounted for radiation by the introduction of a high-Z material. This was explicitly checked in [26]. While early speculation considered plasma dilution by the increased C concentration as a potential candidate to explain the higher P_{LH} in the C-walled AUG [12], the work by Shao *et al* identified changes in the edge density profiles as a key element for the different P_{LH} [26]. In this work it was shown that with the W wall the L-mode electron edge density is higher at the pedestal top location and exhibits a steeper edge gradient compared to the n_e profile in the C-walled AUG. This leads to an intrinsically larger logarithmic edge density gradient $1/L_{n_e}$ in a W compared to a C wall machine. The reasons for the changes in the edge density profiles arise from different divertor detachment conditions combined with a higher recycling coefficient for W, since a larger number of energetic particles is reflected from the metal wall [68].

Furthermore, in the work by Shao *et al* it was also found that in both W and C wall AUG the same minimum value of E_r is obtained at the L–H transition and that this value is very similar to those deduced by Sauter *et al* [14] and later by Cavedon *et al* [36]. With similar assumptions as made in [14], these observations indicate that the same critical E_r gradients have to be established at the L–H transition in both C- and W-walled machines. Combining this result with the observed larger logarithmic edge density gradient $1/L_{n_e}$ in the W compared to the C wall, recalling that if $n_e = n_i$ is assumed $1/L_{n_e}$ enters E_r via $(\nabla_r p_i)/(Z_i e n_i)$ (see equation (2)), gives an explanation for the reduced P_{LH} in a W-walled machine. With an intrinsically higher density gradient less heating power is needed to establish the same T_i and, thus, E_r gradients needed for the H-mode access. This result demonstrates that E_r and its related local quantities are fundamentally connected to the L–H transition physics and can unify observations made on a macroscopic scale.

4.2. Magnetic perturbations

To avoid already the first ELM, it might be necessary to apply MPs already prior to and during the L–H transition. For this reason it is important to understand how the MPs influence P_{LH} and act on the edge quantities important for the L–H transition. In experiments on different tokamaks [10, 60–66] it has been found that P_{LH} increases with increasing amplitude of the applied MPs, where also a threshold behavior is observed, and that P_{LH} can be increased by a factor of two compared to the value without MPs.

AUG is equipped with two rows of MP coils, which can produce perturbations with a toroidal mode number n up to 4 [69]. Therefore, also at AUG extensive L–H transition studies with MPs have been conducted in the past years. For the L–H transition experiments at AUG resonant and non-resonant $n = 2$ perturbations have been applied, since $n = 2$ perturbations are effective for ELM suppression in H-mode [70]. Initial experiments at AUG showed that the effect of P_{LH} by MPs depends on the density [12, 71]. In the low density branch, up to the

density minimum, P_{LH} was not affected by the MPs. With increasing density, however, P_{LH} increased by up to 20% with the application of MPs. For these experiments a relative perturbation strength of $\partial B_r/B_\phi = 1.2\text{--}1.4 \times 10^{-4}$ at the $q = 5$ magnetic surface was used.

More recent experiments [39] employed MPs with larger relative perturbation amplitudes by lowering the toroidal magnetic field strength and increasing the current in the MP coils. These experiments show that P_{LH} also increases at low density ($\bar{n}_e \approx 3.5 \times 10^{19} \text{ m}^{-3}$), if a critical value of about $\partial B_r/B_\phi = 1.7\text{--}2.0 \times 10^{-4}$ is exceeded. This result is in line with observations of other tokamaks [10, 61, 63–65]. Furthermore, it is found that the increase in P_{LH} depends on the alignment of the MP field, set by the differential phase angle $\Delta\varphi_{\text{UL}}$ between the MP field from the upper coil set and the lower coil set. Figure 7 shows that P_{LH} can increase up to 80% for $\Delta\varphi_{\text{UL}} = 135^\circ\text{--}180^\circ$. This alignment of the MPs at highest P_{LH} differs from the equilibrium field alignment. The same alignment is required to suppress ELMs in H-mode, but the relative radial magnetic field perturbation required to sustain ELM suppression at AUG is below the critical value for the increase of P_{LH} . These might be promising results for ITER, as in AUG ELM suppression can be sustained without a simultaneous increase of the H-mode power threshold.

Linear resistive single fluid magneto-hydrodynamic (MHD) calculations using MARS-F [72] were performed to interpret these experimental results. They show a correlation of P_{LH} with the resonant component of the radial field perturbation, represented by the normalized quantity b_{res}^1 [73] and calculated at the $m = nq = 10$ rational surface (m is the poloidal mode number). This correlation is depicted in figure 7 and it shows that b_{res}^1 including the plasma response (solid blue line) is required to predict the $\Delta\varphi_{\text{UL}}$ needed to increase P_{LH} . Calculations using only the vacuum field (dashed blue line) are not able to predict the dependence on $\Delta\varphi_{\text{UL}}$ correctly. Furthermore, the inclusion of a critical magnetic field perturbation strength of $\partial B_r/B_\phi = 1.7\text{--}2.0 \times 10^{-4}$ in the linear MHD calculations improves significantly the reproduction of the behavior of P_{LH} with the radial field perturbation (solid red line) [39].

As discussed before (see section 2.2), one explanation for the L–H transition is that the $E \times B$ velocity shear suppresses turbulent transport in the plasma edge. Previous studies at several tokamaks [61–63, 74, 75] suggested that the application of externally applied MPs induces ergodization of the magnetic field at the plasma edge in L-mode, which leads to a reversal and flattening of the E_r gradients. Hence, within this picture, MPs impede access to H-mode via their impact on the edge radial electric field profile. Another possible explanation is that turbulent transport increases in the presence of MPs, which leads to a flattening of the edge kinetic profiles, which then reduces the shear in $v_{E \times B}$ [71]. Both effects could also play together, as experimental observations and simulations on MAST indicate [75–78].

The first L–H transition studies with MPs at AUG showed that the application of MPs leads to a flattening of the edge

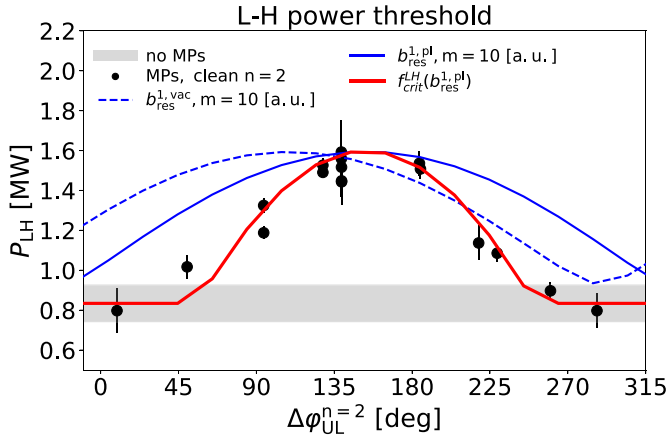


Figure 7. P_{LH} versus the MP field alignment $\Delta\varphi_{UL}$. P_{LH} is highest when the radial field perturbation b_{res}^1 maximizes. Reproduced from [39]. CC BY 4.0.

pressure gradient profile, mainly due to a flattened temperature profile [71]. Consequently, more heating power is needed to achieve the same gradients in edge pressure profiles and, thus, the same $E \times B$ flow shearing rate at the L–H transition. Direct E_r measurements were not available for this data-set, thus, the E_r gradient was approximated by the minimum of the ion or electron pressure gradient, which exhibited values between -7 and -12 kV m^{-1} at the L–H transition both with and without MPs, for different plasma densities and toroidal magnetic field strengths. These values are in good agreement with the observed constant minimum in $v_{E \times B}$ in other L–H transition experiments at AUG [36].

The first comparisons of E_r behavior in AUG between plasmas with and without MPs were performed in low density L-mode plasmas ($n_e \approx 2.0 \times 10^{19} \text{ m}^{-3}$) using DR measurements [79]. In this work by Conway *et al* a reversal of the negative E_r well in the confined region to positive values, i.e. $v_{E \times B}$ changes from the electron diamagnetic to the ion diamagnetic (IDD) drift direction, was observed, consistent with observations in other tokamaks [61–63, 75, 76]. This reversal depends both on the strength of the applied MPs and their resonances with the edge rational surfaces. Furthermore, a dependency of the E_r profile on the absolute MP field orientation was found, which was different in the edge region compared to the SOL. The authors suggested that this could be related to the production of an ergodic layer in the edge region, whereas the SOL remains laminar [79].

A possible correlation of the E_r reversal with the increase of P_{LH} was not investigated in these original experiments, but it has been revisited recently in [39]. In the work by Willensdorfer *et al* the edge E_r and $v_{E \times B}$ profiles were measured with DR, CXRS and HES in L-modes with and without $n=2$ MPs. These experiments were performed at slightly higher densities of about $3.3 \times 10^{19} \text{ m}^{-3}$, with the maximum perturbation amplitude $\partial B_r / B_\phi = 3.0 \times 10^{-4}$ and the MP configuration such that P_{LH} is highest, i.e. $\Delta\varphi_{UL} \approx 135^\circ$ (see also figure 7). Although the toroidal phase angle was varied, the $v_{E \times B}$ profiles did not exhibit a toroidal asymmetry. However,

in all cases in which the MPs led to an increase of P_{LH} the edge $v_{E \times B}$ profiles were elevated at the L–H transition with respect to the reference L-modes without MPs, i.e. the $v_{E \times B}$ profiles were shifted towards the IDD direction. The shear in $v_{E \times B}$, however, was found to be comparable to the one measured at the L–H transition without MPs. These measurements show that the minimum of $v_{E \times B}$ (E_r) is not always a valid proxy for its shear (gradient), but they are consistent with the idea of a critical value of the $v_{E \times B}$ shear (the E_r gradient) required at the L–H transition.

In L-modes the edge $v_{E \times B}$ profile is flatter in plasmas with MPs than in those without. As a result, more heating power is necessary in L-modes with MPs to get a steepening of the $v_{E \times B}$ shear via ∇T_i to values comparable to the ones in L-modes without MPs. Moreover, the additional heating power increases T_e , which reduces the plasma resistivity and, thus, the possible penetration of the MPs. In an L-mode experiment where the field perturbation was slowly ramped up, it was observed that $v_{E \times B}$ reverses at a perturbation of about $\partial B_r / B_\phi = 1.9 \times 10^{-4}$. Since this perturbation amplitude is about the same as that needed to see an increase in P_{LH} , these two phenomena appear to be connected. Furthermore, it was observed that the $v_{E \times B}$ reversal occurs on a faster timescale (within 70 ms) than the ramp-up of the MP perturbation. These observations were tested against several models, which are able to predict a reversal of the $v_{E \times B}$ profile in the presence of MPs. It was found that neoclassical toroidal viscosity cannot explain the flow reversal into the IDD drift direction, because it predicts an additional flow into the electron diamagnetic drift direction. Ergodization as well as resonant electromagnetic torque may partly explain the observations, but more sophisticated modeling including non-linear two-fluid MHD effects together with a more realistic magnetic geometry would be needed for a quantitative comparison.

Finally, MPs have also been observed to change the power threshold for I-mode access [80]. The I-mode is typically observed in unfavorable drift configuration and represents a transitional regime between L-mode and H-mode [81, 82]. It features H-mode-like energy confinement with an edge temperature pedestal, coupled with L-mode-like particle transport and L-mode-like edge density profiles. The I-mode regime itself has also been studied extensively at AUG in the past years, the interested reader is referred to [82–85], but here and in the following only observations prior to and the conditions at the transition from L- into I-mode (L–I transition) and from I- to H-mode (I–H transition) are presented. There are indications that also at the L–I transition the ion channel plays a more important role than the electron channel [80], similar to the observations made in favorable drift configuration plasmas at the L–H transition (see section 2). Experiments using $n=2$ MPs demonstrate an increase in the L–I power threshold related to the flattening of the edge pressure gradient [80]. With MPs more heating power is required to re-establish the same edge pressure gradient, as found at the L–I transition without MPs. These results are reminiscent of the observations made in favorable drift plasmas demonstrating the important role of $v_{E \times B}$ for the L–H transition (see section 2) and suggest

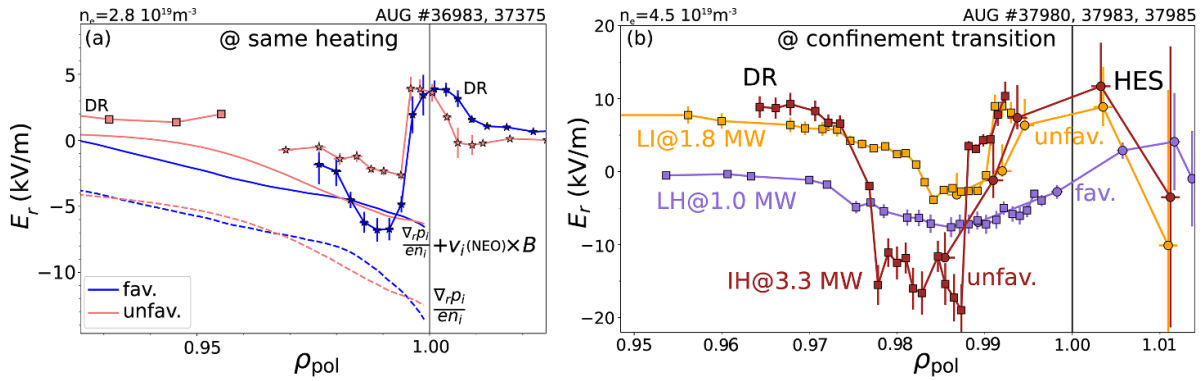


Figure 8. (a) Measured edge radial electric field profiles (stars) in L-modes at matched plasma parameters of favorable (blue) and unfavorable (red) drift configuration. Although $(\nabla_r p_i)/(Z_i e n_i)$ (dashed lines) is the same for both drift configurations, the E_r well is shallower in unfavorable compared to favorable drift configuration. Taking into account the main ion flows, inferred from local neoclassical theory, into the predictions of E_r (solid lines) can also not reproduce the differences observed in the measured E_r profiles. (b) E_r profiles measured with HES (circles) and DR (squares) at the L–H (violet), L–I (orange) and I–H (dark red) transition exhibit different $E_{r,min}$ values and different E_r gradients at the respective confinement transition.

that at least to some extent similar physics mechanisms are at play in the development of an improved confinement in general, independent of the exact magnetic configuration.

4.3. Magnetic configuration

In this section we present findings from AUG regarding H-mode access in different magnetic configurations, concentrating on the favorable and unfavorable drift configurations. At AUG it has been observed that both the power threshold to enter I-mode from L-mode (P_{LI}) as well as the one to enter H-mode from the I-mode (P_{IH}) are larger than P_{LH} [80]. Similar to P_{LH} a parabolic dependence on plasma density is found for P_{LI} , whereas P_{IH} does not exhibit a clear minimum at AUG [27, 80] and other machines [86]. On the other hand, P_{LI} only exhibits a very weak dependence on B_ϕ , whereas P_{IH} increases almost linearly with B_ϕ , similar to P_{LH} . This has been seen most clearly at Alcator C-Mod [86], but is also consistent with the AUG results for a much more limited range of magnetic field strengths [80, 82].

In the work of Ryter *et al* power balance analysis showed that the edge ion heat flux at the L–I transition increases linearly with plasma density. This indicates that the ion channel is also important for the I-mode access, similar as for the L–H transition in favorable drift configuration [80]. However, a quantitative comparison shows that $Q_{i,edge}$ at the L–I transition is higher than $Q_{i,edge}$ at the L–H transition, indicating that the condition to enter I-mode, and also H-mode, in unfavorable drift configuration is different to the condition to enter H-mode in favorable drift configuration. In the framework of edge turbulence suppression by shear flows (see section 2), this observation could indicate a change in the edge turbulence level or the strength of the stabilizing shear flow.

In a recent work at AUG, measurements of edge kinetic profiles and E_r were compared in favorable and unfavorable drift configuration L-modes, for same heating powers and matched plasma densities [27]. It was found that the E_r well at the very

edge of the confined plasma is less pronounced in unfavorable drift configuration compared to favorable drift configuration, although the edge main ion pressure gradient is the same. These features can be seen in figure 8. This shallower E_r well in unfavorable compared to favorable drift configuration has been observed before at AUG [87, 88] and other machines [89, 90], but could now be confirmed with new and improved E_r measurement techniques [27].

No significant changes in the upstream SOL- E_r were found between the two drift configurations, which indicates that the altered H-mode power threshold is not directly connected to changes of SOL quantities with the drift direction. This is also confirmed by indirect measurements of the parallel SOL flows, which are considered to set a boundary condition for the intrinsic toroidal edge rotation [91]. At AUG the intrinsic toroidal edge rotation is of the same size and in the same direction for both drift configurations. Therefore, the explanation for the increased H-mode power threshold in unfavorable drift configuration given in [91] cannot explain the AUG data.

While the positive E_r gradient across the separatrix is of comparable size between the two drift configurations, the shallower E_r well inside the separatrix leads to a weaker (negative) E_r gradient in the confined plasma and, thus, to a weaker $\omega_{E \times B}$. This is also shown in figure 8(a). E_r profiles were also calculated using the radial force balance equation (see equation (2)) with neoclassical estimates of the main ion flows. This procedure utilizes the measurement of the impurity toroidal rotation to obtain the one of the main ions. The E_r profiles estimated by this procedure (solid lines in the figure) cannot reproduce the differences observed in E_r (symbols) between favorable and unfavorable configuration plasmas. This indicates that non-neoclassical effects are at play, which change the equilibrium E_r profile and its related $E \times B$ shear in L-mode and could, thereby, alter the condition for the H-mode onset.

In addition to measurements in L-modes at matched conditions, the radial electric field just prior to changes in confinement regime were also studied in [27]. E_r profiles measured

about 20 ms before the I-mode or H-mode onset show that the E_r gradients can be quite different at the respective confinement transitions. The steepest E_r gradients are found at the I–H transition, since the E_r gradients steepen during I-mode as the ion temperature pedestal evolves. The shear levels observed at the I–H transition can be even larger than those at the L–H transition observed in favorable configurations.

For the L- to I-mode transition no clear criterion in the edge radial electric field or its shear is found. Measurements of the E_r gradients at the L–I transition can be weaker, steeper, or of the same size as observed at the L–H transition in favorable configuration. In contrast, as discussed in section 2.3, the $E \times B$ shear is observed to be quite constant at the L–H transition in favorable configuration over a wide range of plasma parameters. The measurements of E_r at the L–I and I–H confinement transitions in unfavorable drift clearly demonstrate that it is not a simple single-value threshold in $\omega_{E \times B}$, which is required for the access to an improved confinement, but rather indicates that with the drift configuration also other parameters important for the L–H transition must change, such as the characteristics of the edge turbulence.

It should be noted that these observations do not exclude that close to the L–H transition also additional fluctuating shear flows, like zonal flows (ZFs) [92, 93], could become important and even trigger the transition into H-mode. A characterization of such a turbulence–flow interaction close to the L–H transition at AUG has been reported and is also introduced in section 5.2. However, the high reproducibility of the L–H transition also indicates that the gradients of the background profiles, like the main ion pressure and the equilibrium E_r , must be already close to a critical threshold value, in order to establish that the transition into the improved confinement regime occurs always at the same input power for plasma discharges of identical plasma configuration.

5. L-mode turbulence properties and interaction with shear flows close to the L–H transition

In addition to investigating the nature of the stabilizing $E \times B$ shear flow, also the L-mode edge turbulence has to be characterised to fully understand the process leading to the L–H transition. In the past years, several advances in theoretical work have been achieved on this topic by the AUG team, where it was found that the modeling capabilities of gyro-kinetic codes have to be extended close to or across the separatrix in order to capture the phenomena of the L–H transition correctly [94–96]. Experimental work closely linked to theoretical considerations that focused on the characterization and determination of edge turbulence close to and at the L–H transition was also performed.

5.1. L–H–L separation through the separatrix operational space

In a recent study by Eich and Manz the conditions for the L–H transition as well as for the density limits have been related

to separatrix conditions and the characteristic edge turbulence in AUG [97]. In this experimental framework, which has also been discussed e.g. by LaBombard *et al* for Alcator C-Mod data [91], the boundaries for tokamak operation are determined by properties of interchange-drift-Alfvén turbulence at the separatrix. In this way the L–H transition condition as well as the density limits can be written as a combination of several dimensionless separatrix parameters and occur as boundaries in the operational space of the AUG tokamak. In practice, this translates to an existence diagram in terms of separatrix electron density, $n_{e,sep}$, and temperature, $T_{e,sep}$, as shown in figure 9.

According to this model the L-mode edge turbulence close to the density limit ($n_{e,sep} > 2.8 \times 10^{19} \text{ m}^{-3}$), i.e. also close to the H–L back transition, is expected to be in the regime of resistive ballooning mode turbulence, with high electron turbulent transport levels and a flattened pressure gradient. On the other hand, typical low density L–H transition experiments in AUG are expected to occur in the regime of drift-wave-dominated turbulence, where the electron turbulent transport level is rather moderate in the preceding L-mode. In the context of this model the transition into H-mode is observed when the energy transfer from the turbulence to the mean flow, via Reynolds stress, exceeds the energy input to the turbulence, which is given through the measured gradients in the edge kinetic profiles. Thus, the criterion for the L–H transition is also given by turbulence suppression through stabilizing shear flows (see also equation (8) in [97]). The picture is similar to the model developed by Kim and Diamond for the ZF generation by turbulence [98]. In the model developed by Eich and Manz the interaction between turbulence and shear flow is treated in a similar way to that of the ZF physics, although the equilibrium shear flow is assumed to be dominant [97].

A database consisting of 123 AUG discharges containing 1884 time windows with L- and H-modes of different densities and heating powers shows that the L-mode and H-mode experimental points are well separated by the proposed condition for the L–H transition of the Eich and Manz model (see figure 9). The L–H separation line in the $(n_{e,sep}, T_{e,sep})$ space (blue line) corresponds to a specific combination of I_p and B_ϕ , which were kept constant at 0.8 MA and 2.5 T, respectively, within the data-set displayed. Nevertheless, the condition holds more generally also for other combinations in the full experimental data-set.

Within this framework, also the crucial role of the ion heat channel in the L–H transition, which was previously found experimentally at AUG (see section 2.1) can be understood, as the contribution of the ion channel to the entire edge turbulence is the most relevant one at low densities. It is mainly this contribution to the edge turbulence which has to be suppressed by the $E \times B$ shear flow in order to enter H-mode at low densities. Interestingly, for the H–L back transition, for which the same condition holds, it is found that also the electron channel needs to be taken into account in the turbulence generation. As a result, consistency of this model with experimental observations at AUG is found in the sense that at the

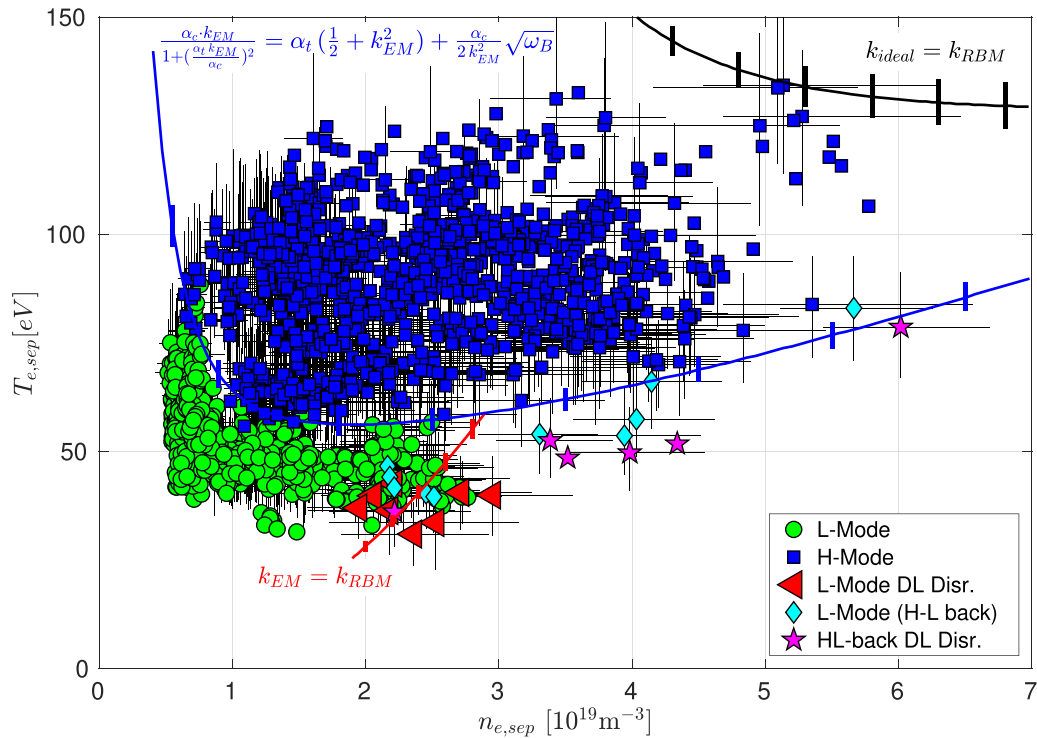


Figure 9. The separatrix operational space of ASDEX Upgrade in terms of separatrix electron density and temperature. The blue line depicts the condition for the L–H (H–L back) transition. Reproduced from [97]. EURATOM 2021. CC BY 3.0.

L–H transition the electron heat flux exhibits a non-monotonic density dependence, as does P_{LH} , whereas the ion heat flux shows a linear dependence on the (separatrix) density (see also figure 5 in [97]).

5.2. Characterization of the I-phase

The I-phase is an intermediate confinement regime that occurs between the L-mode and the fully developed H-mode. The I-phase has been observed in several tokamaks in the past decades including AUG [99, 100], DIII-D [101], COMPASS [102] and EAST [103], see also references in the recent review [93]. Compared to L-mode, the I-phase already exhibits improved particle and energy confinement, although not as high as in type-I ELMy H-modes. The I-phase appears as a sequence of limit-cycle oscillations (LCOs) [99], where edge temperature and density profiles are flattened in periodic bursts or pulses [104], as a consequence of repetitive changes in edge turbulence and transport. As the I-phase forms a link between the L- and fully established H-modes, the understanding of transport changes in this regime is crucial for a full physical picture of the entire L–H–L transition cycle.

During fast L–H and H–L transitions the I-phase can be rather short, showing only a few bursts or pulsations. However, in the right parameter range, the I-phase can be held stable for several seconds, easily exceeding many energy confinement times [105, 106]. Such scenarios provide an excellent opportunity to study turbulence-flow interactions over an extended time period.

Several studies suggest that the I-phase oscillations are produced by a predator-prey-like flow-turbulence interaction [100, 101, 107–110], while other studies find them to be more ELM-like edge oscillations [104, 106, 111–113]. A combination of these two behaviors has also been described in the literature [106, 111, 114] where it was observed that the regular LCO pulsations can evolve into intermittent bursts, characterized as type-III ELMs [115]. Work at AUG has provided experimental evidence that supports both of these interpretations.

In low density I-phases, DR measurements showed the following sequence of events within one LCO period [100, 116]: the turbulence level increases until, at a certain critical threshold, a geodesic acoustic mode (GAM) oscillation is triggered together with a turbulence-driven mean flow, which adds to the equilibrium $E \times B$ flow. The shear of this (combined) flow increases until it is large enough to reduce the turbulence level to a point where the GAM is damped, and a new cycle starts. This leads to the typical predator-prey-like behavior, with an additional threshold for the GAM oscillation. The work by Conway *et al* [100] also provides an existence criterion for this oscillation cycle: The averaged shearing rate of the GAM oscillations has to be comparable or larger than the turbulence de-correlation rate, and also larger than the background $E \times B$ flow shearing rate. If the turbulence de-correlation rate is larger than the GAM flow oscillation, the plasma is in L-mode. If the $E \times B$ flow shearing rate exceeds the turbulence de-correlation, the plasma enters H-mode [100]. The cycle described above is predominantly observed at low

densities. With increasing density the GAMs are reduced by collisional damping [93]. Experimentally, the duty cycle of the LCO is also reduced, making the pulses appear more irregular and burst-like. With increasing heating power the transition from L- to I-phase appears as abrupt confinement change, followed by a more gradual evolution into a fully developed H-mode [100].

This evolution of the I-phase bursts with density and heating power is consistent with the picture of the I-phase presented by Birkenmeier *et al* [106] and other works [112, 114, 116] at AUG, where the I-phase oscillations were identified as type-III ELMs. In the investigated plasmas GAMs were not observed. Due to the utilization of NBI power ramps in these studies, only higher plasma densities could be achieved, which leads to a more effective collisional damping of the GAMs [93]. However, as in [100], it was observed that the I-phase develops with increasing heating power from a state with regular LCOs to a state with intermittent bursts. This evolution of the I-phase is seen both at the L–H transition and, in reversed order, at the H–L back transition. In the work by Birkenmeier *et al* also the magnetic signatures of the I-phase were studied, which showed an up-down asymmetry. A similar structure of the I-phase bursts on the magnetic data was observed in the M-mode at JET [104]. These oscillations could be related to up-down asymmetric parallel flow and current perturbations, as studied experimentally and theoretically in [117]. Also LCO models which additionally take into account MHD effects can reproduce a transition into an intermittent state [118], whereas models based solely on turbulence-flow interaction, like the one in [98], lead to regular LCOs only. However, all these models have in common that the underlying process leading to these LCOs is that these edge instabilities are driven by strong gradients in the edge profiles and they are stabilized by strong shear flows.

High radial and temporal resolution measurements of turbulence, mean and ZFs performed in NBI heated, high density AUG plasmas ($\bar{n}_e > 4.5 \times 10^{19} \text{ m}^{-3}$) close to the L–H or H–L back transition [112, 114] allowed two different plasma phases to be investigated in detail. The first is a transient phase, characterized by L–I–L dithers, which are the back-and forth transition from L-mode into I-phase and vice versa. These L–I–L dithers can be seen on several signals including magnetic measurements and the edge density and temperature and they occur on a time scale of a few ms. The second investigated phase was a stable I-phase with regular LCOs in the kHz (sub-ms) range. Simultaneous measurements of the edge temperature and density gradients, as well as of the $E \times B$ flow shear (approximated by the minimum of $v_{E \times B}$) showed that all quantities develop on the same time scale (time resolution of 250 μs) [112].

Measurements with a time resolution of 100 μs [112] and 1 μs [114] found that during the LCOs the turbulence level and the mean $E \times B$ flow shear are in phase, meaning that the turbulence level is highest when the $v_{E \times B}$ shear is lowest. Furthermore, the analysis of the LCOs in the high density I-phase revealed that at all times $v_{E \times B} \approx v_{\text{dia},i}$, where $v_{\text{dia},i}$ is the diamagnetic velocity of the main ions [112]. This equality implies

that in these experiments the total $E \times B$ flow shear was dominated by the edge main ion gradients and that the ZF amplitude was small compared to neoclassical flows, in agreement with observations at JFT-2M [119] and NSTX [120].

Although the physical picture forming the periodicity of the I-phase is not yet fully resolved and different theories of the details of the transport dynamics exist, it appears that the same quantities and mechanisms leading to the L–H transitions are also of major importance for the I-phase. Common to most explanations of the I-phase, and supported by the turbulence measurements, is the interaction between turbulence-driven transport and the stabilizing effect of the $E \times B$ flow shear. It is a critical interplay between the E_r gradients driving the flow and destabilizing effects like strong edge pressure gradients as the source of mode activity, leading to periodic LCOs. If turbulence dominates, the plasma is in L-mode, whereas the periodicity of the LCOs is broken towards the fully established H-mode, with a strong transport barrier allowing for steep edge gradients. The detailed measurements of turbulence properties and flow shears in such experiments is crucial to improve our understanding of the L–H and the H–L back transition.

6. Conclusions and summary

The ability to access stable, high-confinement operational regimes is key to the success of magnetic confinement fusion reactors. As such, both the experimental and theoretical fusion communities have dedicated considerable time and resources to understanding confinement transitions. These efforts have greatly improved our understanding of the conditions under which such transitions, particularly the L–H transition, occur and have enabled us to extrapolate our knowledge to future machines. However, a fundamental physics-based understanding is still lacking. The AUG team has contributed strongly to the L–H transition research and this paper has attempted to summarize these contributions, putting them into context with respect to one another, but also in comparison to results achieved at other machines.

A very well known feature of the L–H power threshold is that it is non-monotonic as a function of electron density. Experiments at AUG focusing on the low density branch examined the role of the edge ion heat flux and were able to provide a robust explanation for the non-monotonic behavior, unifying both the low- and high density branches, the plasma current scaling observed in the low density branch, and the differences in P_{LH} observed as a function of the heating method used. These experiments showed that a critical value of the edge ion heat flux per particle ($Q_{i,\text{edge}}/n_i$) is needed to enter H-mode, see section 2. At low density, on account of the weaker electron-ion collisional coupling, significantly higher heating power is required when pure electron heating is applied to achieve the required $Q_{i,\text{edge}}/n_i$ needed to enter H-mode, which results in the observed increase in the power threshold at low density. Within the framework of a critical threshold in $Q_{i,\text{edge}}/n_i$ to initiate the L–H transition it is possible to predict the density for which the power threshold is

expected to be minimum in future machines as well as the expected power threshold. When applied to ITER, this scaling produces favorable results, yielding power thresholds that should be attainable for the auxiliary heating systems planned for ITER.

While the observed threshold in $Q_{i,\text{edge}}$ provides a compelling unification of the low- and high density branches of the L–H power threshold, it is unlikely to be directly responsible for the L–H transition. Rather, local edge quantities, such as the gradients of the radial electric field (E_r) and their connected shear flow, are the candidates to be responsible for the transition into H-mode, as they can interact with the edge turbulence. Detailed studies of these edge parameters give insight into how confinement transitions take place and provide key data for validation of theoretical models. The edge ion heat flux is, however, linked to E_r via the ion temperature gradient. Experiments at AUG showed that the minimum of the E_r well, which is a proxy for the much more difficult to measure $E \times B$ shear flow, is constant at the L–H transition for a given magnetic configuration, see section 2.2. These works connected the observation of an ion heat flux threshold to a local edge parameter, and directly support the paradigm of turbulence suppression by $E \times B$ shear flow as the mechanisms initiating the confinement transition.

The connection between the H-mode power threshold (P_{LH}) and E_r was extended to the $E \times B$ velocity shear ($\omega_{E \times B} \propto \max|v_{E \times B}| = |E_{r,\text{min}}/B|$), see section 2.3. Here, it was shown that the maximum of $|v_{E \times B}|$ is constant at the L–H transition over a wide range of electron densities and magnetic field values, explaining the magnetic field dependence of P_{LH} and identifying $v_{E \times B}$ as a more fundamental parameter for the L–H transition than E_r . New results presented in the current publication extend those experiments deeper into the low density branch and show a decrease in the measured maximal $|v_{E \times B}|$ values at the L–H transition, whereas the diamagnetic velocity stays relatively constant. This deviation between diamagnetic and $E \times B$ velocity demonstrates that at low density the contributions of the main ion flows become important and the minimum of $v_{E \times B}$ can not be used as a proxy for its shear anymore. Whether the $v_{E \times B}$ shear itself stays constant could not be addressed in a quantitative manner due to limited radial resolution of the E_r measurements. However, the results obtained comparing confinement transitions in favorable and unfavorable magnetic drift configurations show a larger variation of $|v_{E \times B}|$ and its related shear at the L–H transition, see section 4.3. This observation does not confirm the idea that one single critical value of $\omega_{E \times B}$ is required to enter H-mode, but rather that $\omega_{E \times B}$ has to be set into relation with the edge turbulence properties. The experimental observations on $v_{E \times B}$ at the L–H transition are also supported by recent theoretical work done at AUG showing that the impact of $\omega_{E \times B}$ on the L-mode edge turbulence is strongly non-linear and depends on the background plasma parameters as well as the local turbulence characteristics.

The L–H transition and related plasma quantities have also been explored in plasmas with different main ion compositions, see section 3. In AUG, the power threshold in pure He is similar to the one of pure D plasmas, whereas the threshold

in H plasmas is twice as large. Also $Q_{i,\text{edge}}$ at the L–H transition is increased by a factor of two in H compared to D plasmas, whereas the minimum of the E_r well and its gradients were found to show the same values. Within a simple picture on turbulence–flow interaction one might expect that the $E \times B$ shear required to suppress the characteristic edge turbulence is proportional to its amplitude. Hence, in H one would expect to see a higher $\omega_{E \times B}$ at the transition compared to D. However, this is not what is seen in the experiments and it is also not expected from gyrokinetic simulations. Rather, the experiments show a constant $\omega_{E \times B}$ at the L–H transition, independent of the main ion species composition and the simulations show strongly non-linear behavior with complex interplay between the background plasma parameters, the turbulence properties and the shear level required to impact the turbulence. Since the experimental data show a clear and consistent behavior of $\omega_{E \times B}$ at the L–H transition which applies equally to D and to H plasmas, the observed increase in P_{LH} in H compared to D follows directly from this result: the higher level of turbulence transport in H means more input power is required to reach the critical threshold in $\omega_{E \times B}$.

The L–H power threshold is of high interest for future fusion reactors, not just for reactor operation in D–T, but also for initial commissioning phases, during which they will operate using either hydrogen or helium as the working gas to avoid neutron activation of the machine. Hence the power threshold dependence on the main ion species mix will impact multiple phases of reactor operation. The high power threshold observed in H plasmas is a particular concern for future machines, which have limited amounts of auxiliary heating power capabilities. As such, any methods of reducing the power threshold that can be identified in present experiments are of high interest. Thus, the AUG and JET results demonstrating a 25% reduction in P_{LH} when transitioning from a C-walled to a W-walled device, see section 4.1, are very beneficial for reactor operation. Similarly, the reduction in P_{LH} observed at JET when seeding low levels of He (about 10%) into H plasmas heated with NBI would indicate a promising option for the reactor commissioning phase. However, at AUG similar experiments conducted in both NBI and ECRH heated plasmas did not show any reduction of P_{LH} with a He concentration of up to 20%, see section 3, which indicates that in ITER a reduction of the high H-mode power threshold in H plasmas by He seeding cannot be achieved in the PFPO-1 phase, where only ECRH heating is available. The results from AUG are consistent with recent DIII-D findings, which also show no change in P_{LH} with up to 20% He seeding. Also, in a series of new experiments presented here, the power threshold was explored across the transition from H to D. Similar to the H to He results, no change in the power threshold is observed when seeding H into D plasmas until a 50/50 mix is achieved. Above 50% the power threshold increases smoothly until the twice as high H-mode power threshold of pure H plasmas is reached.

Another concern for future machines is that the use of MPs to suppress ELMs may result in an unforeseen increase in P_{LH} . Early results from AUG showed that at low density no increase in the power threshold was observed with MPs, but

at higher densities an increase of up to 20% was observed. Recent AUG experiments, conducted at the density minimum of P_{LH} , demonstrated that an increase in the power threshold is observed if the MP amplitude is above a critical value. At AUG, the field amplitude needed to suppress ELMs is below that which results in an increase in P_{LH} . This is a potentially very promising result for ITER, as at AUG ELM suppression can be maintained without a simultaneous increase in the H-mode power threshold. Modeling of these experiments shows that the increase in P_{LH} is strongest when the MP is oriented such to maximize the plasma response. The increase in P_{LH} is thought to be due to the changes in the edge $E \times B$ velocity shear, which is reduced in the presence of MPs. Therefore, with MPs more heating power is required to increase the edge gradients and increase the $E \times B$ shear to initiate the L–H transition. Another important observation from these experiments is that the minimum of the $E \times B$ velocity profile is higher with MPs than without. Therefore, also under these conditions, the minimum of $v_{E \times B}$ is not a good representation for its shear.

At AUG the L–H transition has also been investigated recently by connecting the separatrix conditions of n_e and T_e to the edge interchange-drift-Alfvén turbulence properties. The result of this semi-analytical model approach is an existence, or operational space diagram for a large database of AUG L-mode and H-modes. Between the two well separated regimes is an identifiable boundary which can be parameterized in terms of standard plasma parameters. The underlying context of the model is still the suppression of turbulence through equilibrium shear flows. Here the role of ZFs is assumed to be sub-dominant.

The I-phase is an intermediate regime, which occurs at the transition from L-mode to H-mode and at the H–L back transition. However, the I-phase is not a transitory regime, because it can be sustained indefinitely under appropriate conditions. The study of the I-phase and its related plasma edge oscillations, so called LCOs, gives insight into the critical interplay between the stabilizing effects of $E \times B$ shear flows and destabilizing effects, like strong edge pressure gradients, on the edge turbulence. In low collisionality plasmas at AUG the LCOs are associated with turbulence-driven GAMs. With increasing density the regular LCOs evolve to a more sporadic, bursty nature with the same magnetic signatures as type-III ELMs. At AUG the characteristics of the I-phase have been well studied experimentally and also modeled heuristically. However, fully consistent theoretical models over the full I-phase existence parameter space remain outstanding. The reproduction of the I-phase with its characteristic edge oscillations is an important aspect for models seeking to reproduce the L–H transition.

Predicting the L–H transition is a critical issue for the operational success of future magnetic confinement fusion reactors which will operate in improved confinement regimes. Therefore, present-day fusion research devices aim to improve the predictability of the H-mode power threshold under reactor conditions. The AUG team has contributed with experimental and modeling efforts to improve our understanding of the underlying physics mechanisms leading to the L–H transition. Different key parameters have been identified and the

critical role of $v_{E \times B}$ and its related shear have been shown to be important for the H-mode access. On the other hand it is also found that the investigation and characterization of the $E \times B$ shear flow alone is not sufficient to describe all phenomena related to and observed at the L–H transition. The background shear flow has to be brought into a broader context and set in relation with the characteristic edge turbulence, which requires often another level of sophistication. First attempts to address the shear flow-turbulence interaction leading to the L–H transition have been made experimentally and theoretically at AUG, but more comparisons and detailed analysis are foreseen in the near future. This is possible as both the modeling and measurement capabilities are rapidly improving and they are evermore able to capture the different aspects of the L–H transition and the entire concept of shear flow-turbulence interaction correctly.











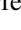
Data availability statement

The data that support the findings of this study are available upon reasonable request from the authors.

Acknowledgments

The authors would like to thank C Angioni, T Pütterich, F Ryter and E Wolfrum for fruitful discussions and valuable input. This work has been carried out within the framework of the EUROfusion Consortium, funded by the European Union via the Euratom Research and Training Programme (Grant Agreement No. 101052200—EUROfusion). Views and opinions expressed are however those of the author(s) only and do not necessarily reflect those of the European Union or the European Commission. Neither the European Union nor the European Commission can be held responsible for them.

ORCID iDs

U Plank  <https://orcid.org/0000-0002-1509-4308>
 R M McDermott  <https://orcid.org/0000-0002-8958-8714>
 G Birkenmeier  <https://orcid.org/0000-0001-7508-3646>
 N Bonanomi  <https://orcid.org/0000-0003-4344-3330>
 M Cavedon  <https://orcid.org/0000-0002-0013-9753>
 G D Conway  <https://orcid.org/0000-0002-3947-4268>
 T Eich  <https://orcid.org/0000-0003-3065-8420>
 M Griener  <https://orcid.org/0000-0003-2953-536X>
 O Grover  <https://orcid.org/0000-0002-7695-8050>
 P A Schneider  <https://orcid.org/0000-0001-7257-3412>
 M Willensdorfer  <https://orcid.org/0000-0002-1080-4200>

References

- [1] Zohm H *et al* 2013 On the physics guidelines for a tokamak DEMO *Nucl. Fusion* **53** 073019
- [2] ITER Organization 2018 *ITER report* ITR-18-003
- [3] Rodriguez-Fernandez P *et al* 2022 Overview of the SPARC physics basis towards the exploration of burning-plasma regimes in high-field, compact tokamaks *Nucl. Fusion* **62** 042003

- [4] Martin Y R and Takizuka T (ITPA CDBM H-mode Threshold Database Working Group 3) 2008 Power requirement for accessing the H-mode in ITER *J. Phys.: Conf. Ser.* **123** 012033
- [5] Takizuka T *et al* 2004 Roles of aspect ratio, absolute B and effective Z of the H-mode power threshold in tokamaks of the ITPA database *Plasma Phys. Control. Fusion* **46** A227
- [6] Connor J W and Wilson H R 2000 A review of theories of the L–H transition *Plasma Phys. Control. Fusion* **42** R1–R74
- [7] Fielding S J, Valovic M, Carolan P G, Gates D A, Hunt C, Leahy P and Morris A W (The COMPASS-D Physics and ECRH Teams) 1998 H-modes on COMPASS-D with high-power ECRH *Plasma Phys. Control. Fusion* **40** 731–5
- [8] Fukuda T, Takizuka T, Tsuchiya K, Kamada Y and Asakura N 2000 Reduction of L–H transition threshold power under the W-shaped pumped divertor geometry in JT-60U *Plasma Phys. Control. Fusion* **42** A289–97
- [9] Andrew Y *et al* 2006 H-mode access in the low density regime on JET *Plasma Phys. Control. Fusion* **48** 479–88
- [10] Gohil P, Evans T E, Fenstermacher M E, Ferron J E, Osborne T H, Park J M, Schmitz O, Scoville J T and Unterberg E A 2011 L–H transition studies on DIII-D to determine H-mode access for operational scenarios in ITER *Nucl. Fusion* **51** 103020
- [11] Ma Y, Hughes J, Hubbard A, LaBombard B, Churchill R, Goufopoulos T, Tsujii N and Marmar E 2012 Scaling of H-mode threshold power and L–H edge conditions with favourable ion grad-B drift in Alcator C-Mod tokamak *Nucl. Fusion* **52** 023010
- [12] Ryter F *et al* 2013 Survey of the H-mode power threshold and transition physics studies in ASDEX Upgrade *Nucl. Fusion* **53** 113003
- [13] David P, Bernert M, Cavedon M, Harrer G F and Eich T (The ASDEX Upgrade Team) 2022 Influence of pedestal radiation on the H–L transition using krypton seeded discharges at ASDEX Upgrade *Nucl. Fusion* **62** 106012
- [14] Sauter P, Pütterich T, Ryter F, Viezzer E, Wolfrum E, Conway G D, Fischer R, Kurzan B, McDermott R M and Rathgeber S K (The ASDEX Upgrade Team) 2012 L- to H-mode transitions at low density in ASDEX Upgrade *Nucl. Fusion* **52** 012001
- [15] Ryter F, Barrera Orte L, Kurzan B, McDermott R M, Tardini G, Viezzer E, Bernert M and Fischer R (The ASDEX Upgrade Team) 2014 Experimental evidence for the key role of the ion heat channel in the physics of the L–H transition *Nucl. Fusion* **54** 083003
- [16] Schmidtmayr M *et al* 2018 Investigation of the critical edge ion heat flux for L–H transitions in Alcator C-Mod and its dependence on B_T *Nucl. Fusion* **58** 056003
- [17] Bilato R, Angioni C, Birkenmeier G and Ryter F (The ASDEX Upgrade Team) 2020 Heuristic model for the power threshold of the L–H transition *Nucl. Fusion* **60** 124003
- [18] Biglari H, Diamond P H and Terry P W 1990 Influence of sheared poloidal rotation on edge turbulence *Phys. Fluids B* **2** 1–4
- [19] Kaye S *et al* 1997 ITER L mode confinement database *Nucl. Fusion* **37** 1303–28
- [20] Gohil P, Jernigan T C, Osborne T H, Scoville J T and Strait E J 2010 The torque dependence of the H-mode power threshold in hydrogen, deuterium and helium plasmas in DIII-D *Nucl. Fusion* **50** 064011
- [21] Waltz R E and Miller R L 1999 Ion temperature gradient turbulence simulations and plasma flux surface shape *Phys. Plasmas* **6** 4265–71
- [22] Rozhansky V and Tendler M 1992 The effect of the radial electric field on the L–H transitions in tokamaks *Phys. Fluids B* **4** 1877–88
- [23] Hinton F L and Hazeltine R D 1976 Theory of plasma transport in toroidal confinement systems *Rev. Mod. Phys.* **48** 239–308
- [24] Kim Y B, Diamond P H and Groebner R J 1991 Neoclassical poloidal and toroidal rotation in tokamaks *Phys. Fluids B* **3** 2050–60
- [25] Rozhansky V, Kaveeva E, Molchanov P, Veselova I, Voskoboynikov S, Coster D, Counsell G, Kirk A and Lisgo S (The ASDEX-Upgrade Team and the MAST Team) 2009 New B2SOLPS5.2 transport code for H-mode regimes in tokamaks *Nucl. Fusion* **49** 025007
- [26] Shao L M, Wolfrum E, Ryter F, Birkenmeier G, Laggner F M, Viezzer E, Fischer R, Willensdorfer M, Kurzan B and Lunt T (The ASDEX Upgrade Team) 2016 On the role of the edge density profile for the L–H transition power threshold in ASDEX Upgrade *Plasma Phys. Control. Fusion* **58** 025004
- [27] Plank U *et al* 2022 Experimental study of the edge radial electric field in different drift configurations and its role in the access to H-mode at ASDEX Upgrade *Phys. Plasmas* submitted
- [28] Viezzer E *et al* 2015 Collisionality dependence of edge rotation and in–out impurity asymmetries in ASDEX Upgrade H-mode plasmas *Nucl. Fusion* **55** 123002
- [29] Viezzer E, Pütterich T, Angioni C, Bergmann A, Dux R, Fable E, McDermott R M, Stroth U, Wolfrum E and The ASDEX Upgrade Team 2014 Evidence for the neoclassical nature of the radial electric field in the edge transport barrier of ASDEX Upgrade *Nucl. Fusion* **54** 012003
- [30] Cavedon M, Dux R, Happel T, Hennequin P, Plank U, Pütterich T, Ryter F, Stroth U, Viezzer E and Wolfrum E (The ASDEX Upgrade Team) 2019 Inner versus outer $E \times B$ shear layer: an attempt to radially localize the L–H transition *Proc. 46th EPS Conf. Plasma Physics (Milan)* p P5.1069
- [31] Bonanomi N, Angioni C, Plank U, Schneider P A and Maggi C F (ASDEX Upgrade Team, EUROfusion MST1 Team and JET Contributors) 2021 Edge turbulent transport toward the L–H transition in ASDEX Upgrade and JET-ILW *Phys. Plasmas* **28** 052504
- [32] Plank U 2021 The effect of the radial electric field around the separatrix on the access to the high confinement mode at ASDEX Upgrade *PhD Thesis* Ludwig-Maximilian University Munich
- [33] Ryter F *et al* 2015 L–H transition physics in hydrogen and deuterium: key role of the edge radial electric field and ion heat flux *Plasma Phys. Control. Fusion* **58** 014007
- [34] Viezzer E *et al* 2013 High-accuracy characterization of the edge radial electric field at ASDEX Upgrade *Nucl. Fusion* **53** 053005
- [35] Maggi C F *et al* 2014 L–H power threshold studies in JET with Be/W and C wall *Nucl. Fusion* **54** 023007
- [36] Cavedon M *et al* 2020 Connecting the global H-mode power threshold to the local radial electric field at ASDEX Upgrade *Nucl. Fusion* **60** 066026
- [37] Cavedon M, Pütterich T, Viezzer E, Dux R, Geiger B, McDermott R M, Meyer H and Stroth U (ASDEX Upgrade Team) 2017 A fast edge charge exchange recombination spectroscopy system at the ASDEX Upgrade tokamak *Rev. Sci. Instrum.* **88** 043103
- [38] Rozhansky V 2004 Understanding transport barriers through modelling *Plasma Phys. Control. Fusion* **46** A1
- [39] Willensdorfer M *et al* 2022 Dependence of the L–H power threshold on the alignment of external non-axisymmetric magnetic perturbations in ASDEX Upgrade *Phys. Plasmas* **29** 032506
- [40] Silva C *et al* 2021 Structure of the JET edge radial electric field in He and D plasmas *Nucl. Fusion* **61** 126006

- [41] ASDEX Team 1989 The H-mode of ASDEX *Nucl. Fusion* **29** 1959–2040
- [42] Righi E *et al* 1999 Isotope scaling of the H mode power threshold on JET *Nucl. Fusion* **39** 309–19
- [43] Stober J *et al* 2020 Exploring fusion-reactor physics with high-power electron cyclotron resonance heating on ASDEX Upgrade *Plasma Phys. Control. Fusion* **62** 024012
- [44] Ryter F *et al* 2009 H-mode threshold and confinement in helium and deuterium in ASDEX Upgrade *Nucl. Fusion* **49** 062003
- [45] McDonald D C *et al* 2004 ELMy H-modes in JET helium-4 plasmas *Plasma Phys. Control. Fusion* **46** 519–34
- [46] Solano E *et al* 2021 L–H transition threshold studies in helium plasmas at JET *Nucl. Fusion* **61** 124001
- [47] Schneider P A, Hennequin P, Bonanomi N, Dunne M, Conway G D and Plank U (The ASDEX Upgrade Team and The EUROfusion MST1 Team) 2021 Overview of the isotope effects in the ASDEX Upgrade tokamak *Plasma Phys. Control. Fusion* **63** 064006
- [48] Plank U, Pütterich T, Angioni C, Bonanomi N, Cavedon M, Conway G, Dux R, Happel T, McDermott R and Schneider P A (The ASDEX Upgrade Team) 2022 Experimental investigations of the H-mode access in mixed hydrogen–deuterium plasmas at ASDEX Upgrade *Proc. 48th EPS Conf. Plasma Physics (Maastricht)* p O1.103 (available at: <http://ocs.ciemat.es/EPS2022PAP/pdf/O1.103.pdf>)
- [49] Birkenmeier G *et al* 2022 The power threshold of H-mode access in mixed hydrogen–tritium and pure tritium plasmas at JET with ITER-like wall *Nucl. Fusion* **62** 086005
- [50] Birkenmeier G *et al* 2022 The power threshold of H-mode access in tritium and deuterium–tritium plasmas at JET with ITER-like wall *Proc. 48th EPS Conf. Plasma Physics (Maastricht)* p I1.102
- [51] Bonanomi N, Angioni C, Crandall P C, Di Siena A, Maggi C F and Schneider P A (The ASDEX Upgrade Team, The EUROfusion MST1 Team and JET Contributors) 2019 Effect of the isotope mass on the turbulent transport at the edge of L-mode plasmas in ASDEX Upgrade and JET-ILW *Nucl. Fusion* **59** 126025
- [52] Belli E A, Candy J and Waltz R E 2020 Reversal of simple hydrogenic isotope scaling laws in tokamak edge turbulence *Phys. Rev. Lett.* **125** 015001
- [53] Belli E A, Candy J and Waltz R E 2019 Reversal of turbulent gyroBohm isotope scaling due to nonadiabatic electron drive *Phys. Plasmas* **26** 082305
- [54] Bonanomi N, Angioni C, Schneider P A, Conway G D, Happel T, Plank U and Staebler G M (The ASDEX Upgrade Team and The EUROfusion MST1 Team) 2022 From L-mode to the L–H transition, experiments on ASDEX Upgrade, gyrokinetic simulations and full-radius transport modeling *Proc. 48th EPS Conf. Plasma Physics (Maastricht)* p O5.101
- [55] Solano E *et al* 2022 Recent progress in L–H transition studies at JET: tritium, helium, hydrogen and deuterium *Nucl. Fusion* **62** 076026
- [56] Plank U *et al* 2020 H-mode power threshold studies in mixed ion species plasmas at ASDEX Upgrade *Nucl. Fusion* **60** 074001
- [57] Hillesheim J *et al* 2018 Implications of JET-ILW L–H transition studies for ITER *Proc. 27th IAEA Fusion Energy Conf. (Gandhinagar)* vol IAEA-CN-258 p EX/4–1
- [58] Schmitz L *et al* 2022 Reducing the L–H transition power threshold ITER-similar-shape DIII-D hydrogen plasmas *Nucl. Fusion* **62** 126050
- [59] Willensdorfer M *et al* 2012 Electron density evolution after L–H transitions and the L–H/H–L cycle in ASDEX Upgrade *Nucl. Fusion* **52** 114026
- [60] Leonard A, Howald A, Hyatt A, Shoji T, Fujita T, Miura M, Suzuki N and Tsuji S (JFT-2M Group) 1991 Effects of applied error fields on the H-mode power threshold of JFT-2M *Nucl. Fusion* **31** 1511–8
- [61] Scannell R, Kirk A, Carr M, Hawke J, Henderson S S, O’Gorman T, Patel A, Shaw A and Thornton A (The MAST Team) 2015 Impact of resonant magnetic perturbations on the L–H transition on MAST *Plasma Phys. Control. Fusion* **57** 075013
- [62] Mordijck S, Rhodes T L, Zeng L, Doyle E J, Schmitz L, Chrystal C, Strait T J and Moyer R A 2015 Effects of resonant magnetic perturbations on turbulence and transport in DIII-D L-mode plasmas *Plasma Phys. Control. Fusion* **58** 014003
- [63] Schmitz L *et al* 2019 L–H transition trigger physics in ITER-similar plasmas with applied $n = 3$ magnetic perturbations *Nucl. Fusion* **59** 126010
- [64] In Y *et al* 2017 Enhanced understanding of non-axisymmetric intrinsic and controlled field impacts in tokamaks *Nucl. Fusion* **57** 116054
- [65] Park H *et al* 2019 Overview of KSTAR research progress and future plans toward ITER and K-DEMO *Nucl. Fusion* **59** 112020
- [66] Kaye S *et al* 2011 L–H threshold studies in NSTX *Nucl. Fusion* **51** 113019
- [67] Neu R *et al* 2007 Operational conditions in a W-clad tokamak *J. Nucl. Mater.* **367–370** 1497–502
- [68] Lunt T, Reimold F, Wolfrum E, Carralero D, Feng Y and Schmid K (The ASDEX Upgrade Team) 2017 Influence of the first wall material on the particle fuelling in ASDEX Upgrade *Plasma Phys. Control. Fusion* **59** 055016
- [69] Suttrop W *et al* 2009 In-vessel saddle coils for MHD control in ASDEX Upgrade *Fusion Eng. Des.* **84** 290–4
- [70] Suttrop W *et al* 2018 Experimental conditions to suppress edge localised modes by magnetic perturbations in the ASDEX Upgrade tokamak *Nucl. Fusion* **58** 096031
- [71] Ryter F, Rathgeber S, Viezzer E, Suttrop W, Burckhart A, Fischer R, Kurzan B, Potzel S and Pütterich T (The ASDEX Upgrade Team) 2012 L–H transition in the presence of magnetic perturbations in ASDEX Upgrade *Nucl. Fusion* **52** 114014
- [72] Ryan D A *et al* 2015 Toroidal modelling of resonant magnetic perturbations response in ASDEX-Upgrade: coupling between field pitch aligned response and kink amplification *Plasma Phys. Control. Fusion* **57** 095008
- [73] Liu Y *et al* 2016 Toroidal modelling of RMP response in ASDEX Upgrade: coil phase scan, q95 dependence and toroidal torques *Nucl. Fusion* **56** 056015
- [74] Coenen J, Schmitz O, Unterberg B, Clever M, Jakubowski M, Samm U, Schweer B, Stoschus H and Tokar M (TEXTOR Team) 2011 Rotation and radial electric field in the plasma edge with resonant magnetic perturbation at TEXTOR *Nucl. Fusion* **51** 063030
- [75] Kirk A, Liu Y, Nardon E, Tamain P, Cahyna P, Chapman I, Denner P, Meyer H, Mordijck S and Temple D (The MAST Team) 2011 Magnetic perturbation experiments on MAST L- and H-mode plasmas using internal coils *Plasma Phys. Control. Fusion* **53** 065011
- [76] Tamain P, Kirk A, Nardon E, Dudson B and Hnat B (The MAST Team) 2010 Edge turbulence and flows in the presence of resonant magnetic perturbations on MAST *Plasma Phys. Control. Fusion* **52** 075017
- [77] Rozhansky V, Kaveeva E, Molchanov P, Veselova I, Voskoboynikov S, Coster D, Kirk A, Lisgo S and Nardon E 2010 Modification of the edge transport barrier

- by resonant magnetic perturbations *Nucl. Fusion* **50** 034005
- [78] Rozhansky V, Molchanov P, Kaveeva E, Voskoboinikov S, Kirk A, Nardon E, Coster D and Tendler M 2011 Modelling of the edge plasma of MAST in the presence of resonant magnetic perturbations *Nucl. Fusion* **51** 083009
- [79] Conway G D, Fietz S, Müller H W, Lunt T, Simon P, Suttrop W, Maraschek M, Happel T and Viezzer E (ASDEX Upgrade Team) 2014 Impact of magnetic perturbation coils on the edge radial electric field and turbulence in ASDEX Upgrade *Plasma Phys. Control. Fusion* **57** 014035
- [80] Ryter F *et al* 2017 I-mode studies at ASDEX Upgrade: L–I and I–H transitions, pedestal and confinement properties *Nucl. Fusion* **57** 016004
- [81] Whyte D G *et al* 2010 I-mode: an H-mode energy confinement regime with L-mode particle transport in Alcator C-Mod *Nucl. Fusion* **50** 105005
- [82] Happel T *et al* 2017 The I-mode confinement regime at ASDEX Upgrade: global properties and characterization of strongly intermittent density fluctuations *Plasma Phys. Control. Fusion* **59** 014004
- [83] Stimmel K, Bañón Navarro A, Happel T, Told D, Görler T, Wolfrum E, Martin Collar J P, Fischer R, Schneider P A and Jenko F (ASDEX Upgrade Team) 2019 Gyrokinetic investigation of the ASDEX Upgrade I-mode pedestal *Phys. Plasmas* **26** 122504
- [84] Silvagni D *et al* 2020 I-mode pedestal relaxation events at ASDEX Upgrade *Nucl. Fusion* **60** 126028
- [85] Manz P *et al* 2015 Geodesic oscillations and the weakly coherent mode in the I-mode of ASDEX Upgrade *Nucl. Fusion* **55** 083004
- [86] Hubbard A *et al* 2016 Multi-device studies of pedestal physics and confinement in the I-mode regime *Nucl. Fusion* **56** 086003
- [87] Schirmer J, Conway G D, Zohm H and Suttrop W (ASDEX Upgrade Team) 2006 The radial electric field and its associated shear in the ASDEX Upgrade tokamak *Nucl. Fusion* **46** S780–91
- [88] Meyer H *et al* 2006 H-mode physics of near double null plasmas in MAST and its applications to other tokamaks *Nucl. Fusion* **46** 64–72
- [89] Carlstrom T N, Groebner R J, Fenzi C, McKee G R, Moyer R A and Rhodes T L 2002 Evidence for the role of velocity shear on the L–H transition in DIII-D *Plasma Phys. Control. Fusion* **44** A333
- [90] Vermare L *et al* 2022 Formation of the radial electric field profile in the WEST tokamak *Nucl. Fusion* **62** 026002
- [91] LaBombard B, Hughes J, Mossessian D, Greenwald M, Lipschultz B and Terry J (The Alcator C-Mod Team) 2005 Evidence for electromagnetic fluid drift turbulence controlling the edge plasma state in the Alcator C-Mod tokamak *Nucl. Fusion* **45** 1658–75
- [92] Diamond P H, Itoh S I, Itoh K and Hahm T S 2005 Zonal flows in plasma—a review *Plasma Phys. Control. Fusion* **47** R35–161
- [93] Conway G, Smolyakov A and Ido T 2021 Geodesic acoustic modes in magnetic confinement devices *Nucl. Fusion* **62** 013001
- [94] Michels D, Ulbl P, Zholobenko W, Body T, Stegmeir A, Eich T, Griener M, Conway G D and Jenko F (ASDEX Upgrade Team) 2022 Full-f electromagnetic gyrokinetic turbulence simulations of the edge and scrape-off layer of ASDEX Upgrade with GENE-X *Phys. Plasmas* **29** 32307
- [95] Zholobenko W, Stegmeir A, Griener M, Conway G D, Body T, Coster D and Jenko F (The ASDEX Upgrade Team) 2021 The role of neutral gas in validated global edge turbulence simulations *Nucl. Fusion* **61** 116015
- [96] Zholobenko W, Body T, Manz P, Stegmeir A, Zhu B, Griener M, Conway G D, Coster D and Jenko F (The ASDEX Upgrade Team) 2021 Electric field and turbulence in global Braginskii simulations across the ASDEX Upgrade edge and scrape-off layer *Plasma Phys. Control. Fusion* **63** 034001
- [97] Eich T and Manz P (The ASDEX Upgrade Team) 2021 The separatrix operational space of ASDEX Upgrade due to interchange-drift-Alfvén turbulence *Nucl. Fusion* **61** 086017
- [98] Kim E J and Diamond P H 2003 Zonal flows and transient dynamics of the L–H transition *Phys. Rev. Lett.* **90** 4
- [99] Zohm H (ASDEX Upgrade Team) 1994 Dynamic behavior of the L–H transition *Phys. Rev. Lett.* **72** 222
- [100] Conway G D, Angioni C, Ryter F, Sauter P and Vicente J (ASDEX Upgrade Team) 2011 Mean and oscillating plasma flows and turbulence interactions across the L–H confinement transition *Phys. Rev. Lett.* **106** 065001
- [101] Schmitz L, Zeng L, Rhodes T L, Hillesheim J C, Doyle E J, Groebner R J, Peebles W A, Burrell K H and Wang G 2012 Role of zonal flow predator-prey oscillations in triggering the transition to H-mode confinement *Phys. Rev. Lett.* **108** 1–5
- [102] Grover O *et al* 2018 Limit cycle oscillations measurements with Langmuir and ball-pen probes on COMPASS *Nucl. Fusion* **58** 112010
- [103] Shao L M *et al* 2018 Small amplitude oscillations before the L–H transition in EAST *Plasma Phys. Control. Fusion* **60** 035012
- [104] Réfy D I *et al* 2020 Identity of the JET M-mode and the ASDEX Upgrade I-phase phenomena *Nucl. Fusion* **60** 056004
- [105] Conway G D, Angioni C, Poli E, Ryter F, Sauter P, Scott B, Happel T and Vicente J (The ASDEX Upgrade Team) 2010 Behaviour of mean and oscillating $E \times B$ plasma flows and turbulence interactions during confinement mode transitions *Proc. IAEA Fusion Engineering Conf. (Daejeon)* vol IAEA-CN-180 p EXC/7–1
- [106] Birkenmeier G *et al* 2016 Magnetic structure and frequency scaling of limit-cycle oscillations close to L- to H-mode transitions *Nucl. Fusion* **56** 086009
- [107] Moyer R A, Tynan G R, Holland C and Burin M J 2001 Increased nonlinear coupling between turbulence and low-frequency fluctuations at the L–H transition *Phys. Rev. Lett.* **87** 2–5
- [108] Colchin R J *et al* 2002 Slow L–H Transitions in DIII-D Plasmas *Phys. Rev. Lett.* **88** 4
- [109] Xu G S *et al* 2011 First evidence of the role of zonal flows for the L–H transition at marginal input power in the EAST tokamak *Phys. Rev. Lett.* **107** 1–5
- [110] Yan Z, McKee G R, Fonck R, Gohil P, Groebner R J and Osborne T H 2013 Observation of the L–H confinement bifurcation triggered by a turbulence-driven shear flow in a tokamak plasma *Phys. Rev. Lett.* **112** 1–5
- [111] Colchin R J *et al* 2002 Physics of slow L–H transitions in the DIII-D tokamak *Nucl. Fusion* **42** 1134–43
- [112] Cavedon M, Pütterich T, Viezzer E, Birkenmeier G, Happel T, Laggner F M, Manz P, Ryter F and Stroth U (ASDEX Upgrade Team) 2017 Interplay between turbulence, neoclassical and zonal flows during the transition from low to high confinement mode at ASDEX Upgrade *Nucl. Fusion* **57** 014002
- [113] Solano E R *et al* 2017 Axisymmetric oscillations at L–H transitions in JET: M-mode *Nucl. Fusion* **57** 022021
- [114] Medvedeva A, Bottureau C, Clairet F, Hennequin P and Stroth U (The ASDEX Upgrade Team) 2017 Density profile and turbulence evolution during L–H transition studied with the ultra-fast swept reflectometer on ASDEX

- Upgrade *Plasma Phys. Control. Fusion* **59** 125014
- [115] Zohm H 1996 Edge localized modes (ELMs) *Plasma Phys. Control. Fusion* **38** 105–28
- [116] Müller S H *et al* 2014 Direct observations of L–I–H and H–I–L transitions with the X-point reciprocating probe in ASDEX Upgrade *Phys. Plasmas* **21** 042301
- [117] Manz P *et al* 2016 Poloidal asymmetric flow and current relaxation of ballooned transport during I-phase in ASDEX Upgrade *Phys. Plasmas* **23** 052302
- [118] Constantinescu D, Dumbrajs O, Igochine V, Lackner K, Meyer-Spasche R and Zohm H (ASDEX Upgrade Team) 2011 A low-dimensional model system for quasi-periodic plasma perturbations *Phys. Plasmas* **18** 062307
- [119] Kobayashi T *et al* 2013 Spatiotemporal structures of edge limit-cycle oscillation before L-to-H transition in the JFT-2M tokamak *Phys. Rev. Lett.* **111** 1–5
- [120] Diallo A, Banerjee S, Zweben S and Stoltzfus-Dueck T 2017 Energy exchange dynamics across L–H transitions in NSTX *Nucl. Fusion* **57** 066050